

# NICMOS Coronagraphic Imaging Strategy

---

A.B. Schultz, A.D. Storrs, and D. Fraquelli  
August 27, 1999

---

## ABSTRACT

*A set of NICMOS Camera 2 coronagraphic data (SMOV program ID: 7052) are available for use as reference images. The data were obtained to measure the diffractive energy rejection and scattering properties of the coronagraph. The calibration star BD+032964 (G2V) was observed on 1997 July 23 and was stepped at 0.0185 and 0.3 arcsecond steps across the coronagraphic hole in both the image x- and y-axis directions. In addition, observations were obtained at two different S/C roll angles. Subtraction of the images indicates the necessity for positional accuracy of targets to better than 1/8 pixel (~0.009 arcseconds) for PSF subtraction. In addition, a review of coronagraphic observations was performed for program 7227 (GTO/NIC) for which the telescope was rolled in the same orbit. We conclude the best strategy for PSF subtraction for objects close to a bright source (<1.125 arcsec) is to observe the same target in the same orbit with a roll of the spacecraft between observations. This procedure will work if the telescope attitude history is favorable. Rolling the telescope in consecutive orbits will otherwise give equivalent results, and gives as good results if you are looking for extended object or point sources relatively far from the primary source.*

---

## 1. Introduction

NICMOS offers an infrared coronagraphic observing mode with Camera 2. During the observational lifetime of NICMOS, twenty observing programs (including SMOV, GO, GTO, ENG, CAL, and SNAP programs) obtained a total of 3,562 coronagraphic observations. There were 299 onboard ACQs (Mode-2) and 30 acquisitions of bright targets using a variation of the Reuse Target Offset (RTO) capability (Mode-1). A review of the SMOV program 7052 data is presented here to assist the coronagraphic observer and/or archival user with data reduction and to present a synopsis of coronagraphic observing strategies.

Coronagraphic imaging capability is provided by a hole in the Camera 2 Field Divider Assembly (FDA) mirror which is combined with a cold mask at the pupil (Lyot stop). When re-imaged through the Camera 2 f/45 optics, this provides a 0.3 arcsec radius coronagraphic spot, with an effective useful radius of 0.4 arcsec at the detector image plane. Internal cold baffling screens out residual thermal radiation from the edges of the HST primary and secondary mirror and the secondary mirror support structures (pads, spider, and mounts).

## 2. Coronagraphic Acquisition

Coronagraphic imaging requires an acquisition sequence at the beginning of the visit to center the target in the coronagraphic hole. The size of the coronagraphic hole is smaller than typical HST blind-pointing errors. The procedure for a coronagraphic acquisition is to first image the target in Camera 2 using blind-pointing and then use either an onboard, reuse target offset, or interactive acquisition to acquire the target. A slew is calculated and the telescope commanded to move the image of the target over the position of the hole.

For Science Mission Orbital Verification (SMOV) program 7052, flat field and background images of equal exposure times were executed in visit 21 and sent to the ground for analysis before the coronagraphic verification observations, visits 22 and 23. This allowed a measurement of the hole position and a correction to the position of the hole to be uploaded to the S/C. Presumably, the hole would remain stationary during the execution of 7052.

The target star BD+032964 (G2V) was observed on 1997 July 23. It was acquired with an onboard acquisition followed by images of the target in the hole and with the target moved in 0.0185 and 0.3 arcsecond steps (1/4 and 4 pixel steps respectively) across the coronagraphic hole along both the image x- and y-axis. The star was re-acquired at the start of each orbit. In addition, observations during visit 23, orbit 5, were obtained at a different S/C roll angle than was used for visit 22. The time line for visits 22 and 23 are presented in Table 1.

## 3. Calibrating the Data

The data were re-calibrated using the STSDAS task **calnica**. New calibration reference files were used for DARKFILE, NLINFILE, and PHOTTAB. Due to the movement of the coronagraphic hole, a ground thermal vacuum test flat field reference file was used for FLATFILE calibration. The on-orbit flat field reference files have the image of the coronagraphic hole close to the location of the hole in the 7052 data, while for the ground flat, the image of the hole is far from the current location of the hole. The calibration switches BACKCALC and WARNCALC are not yet implemented and were skipped.

### *Pedestal Removal*

“Pedestal” is the residual bias remaining after subtracting a dark reference file. This residual bias when multiplied by the reference flat field, which is inverted, adds a multiple of the inverse sensitivity of the array to the data. A number of groups have developed code for detecting and removing the pedestal from data. The code developed by Roeland van der Marel, Space Telescope Science Institute (STScI), was used to remove pedestal from this data. This software comes without guarantee and on an ‘as is’ basis. It is not being actively maintained or upgraded. (<http://sol.stsci.edu/~marel/software.html>)

**Table 1.** SMOV Program 7052 Visit 22 and 23 Time Line.

Visit	Orbit	LINENUM	OBSMODE	TIME-OBS	Comments
22	1	110	ACQ	03:19:45	First orbit, F187N
		115	MULTIACCUM	03:21:17	F187N filter observation
		120	MULTIACCUM	03:30:05	F110W filter observation
		130	MULTIACCUM	03:32:50	start 0.0185” step X-dither, F160W
			SAA passage		4:18 to 4:26 UT
	2	210	ACQ	04:54:39	Second orbit, F187N
		215	MULTIACCUM	04:56:11	F187N filter observation
		220	MULTIACCUM	05:04:59	F110W filter observation
		230	MULTIACCUM	05:07:44	start 0.0185” step Y-dither, F160W
			SAA passage		5:44 to 6:10 UT
	3	310	ACQ	06:31:29	Third orbit, F187N
		315	MULTIACCUM	06:33:00	F187N filter observation
		320	MULTIACCUM	06:41:49	F110W filter observation
		330	MULTIACCUM	06:44:34	start 0.3” step X-dither, F160W
			SAA passage		7:23 to 7:52 UT
	4	410	ACQ	08:08:16	Fourth orbit, F187N
415		MULTIACCUM	08:09:48	F187N filter observation	
420		MULTIACCUM	08:18:36	F110W filter observation	
430		MULTIACCUM	08:21:21	start 0.3” step Y-dither, F160W	
		SAA passage		9:02 to 9:33 UT	
23	5	510	ACQ	09:46:59	Fifth orbit, roll S/C, F187N
		515	MULTIACCUM	09:48:31	F187N filter observation
		520	MULTIACCUM	10:14:26	F160W filter observation

Visit	Orbit	LINENUM	OBSMODE	TIME-OBS	Comments
		530	MULTIACCUM	10:23:14	F110W filter observation

An IRAF script file (dovdmped.cl) was used to interface to van der Marel's code which sets up the parameter file, extracts the name of the flat field from the science header, creates a bad pixel mask file, and executes the code. The default parameters for van der Marel's pedestal removal code worked quite well for the 7052 data (1997 July 23). The algorithm to fit between quadrant boundaries was skipped. The code parameters that were used to remove pedestal from the 7052 data are listed in Table 2. The task **pedsky**, subtract "pedestal" and sky from an image, is available in STSDAS for data reduction.

**Table 2.** NICMOS Pedestal Removal Parameters (van der Marel).

	Function	Comments
Fitting choice	2	Yes, best-fitting pedestal for all quadrants together
Algorithm	3	Yes, trial - median filtered trial
Quick and dirty	0	No, not appropriate for high accuracy work
Achieve continuity (Iflat)	0	No, do not make quadrants boundaries continuous
Use default parameters	1	Yes
Flat rootname		Give name of the flat field image
Image rootname		Give name of image
Read a mask file	1	Use a mask file to ignore suspect pixels
Clip sci data for mask	4.0	Value above which to clip sci data for mask

The images of the stellar PSF in the coronagraphic images of the 7052 data fill the quadrant with the coronagraphic hole and spills over into adjacent quadrants. This constrains the determination of the pedestal contribution in that quadrant. A mask file was created to flag bright pixels (threshold limit= 4.0 cts/sec) for all pixels. The flagged pixels were not used for estimating the pedestal contribution.

### ***Removing bad pixels, artifacts, etc....***

Identified bad pixels, whether hot or "grot" affected, and many of the camera artifacts, can be removed from the images. However, due to the time involved in identifying and interpolation of these pixels from the data, this reduction step was skipped. A future ISR will describe in detail a procedure that can be used to perform this task.

### *Removing the vertical bands*

The vertical bands (“Mr. Staypuft” effect) emanating from the center of the coronagraphic hole and reflected electronically into adjacent quadrants were removed by subtracting a mask image containing the vertical bands. This mask image was created by averaging the first 19 rows of the image (**blkavg**) and block replicating (**blkrep**) this 1-dimensional image into a 2-dimensional image. The first 19 rows were the only area of the image that was not intersected by the bright diagonal diffraction spike emanating from the hole. In addition, the first 19 rows contain regions vignetted by the Field Offset Mechanism (FOM) and do not sample the sky. The first ~10 rows at the bottom of the image are permanently vignetted while additional rows, up to about 50 rows, become vignetted due to movement of the FOM. The vignetted rows are largely affected only by the electronic noise. For example, the following are captured IRAF screen messages while creating the mask file:

```
> blkavg n45j22ilmB.imh[1:256,1:19] n45j22ilmB_line01 op=ave
blocking factor in dimension 1 (x or column) (1:) (1): 1
blocking factor in dimension 2 (y or line) (1:) (121): y
Warning: Image header parameter not found (CTYPE1)
Warning: Image header parameter not found (CTYPE2)

> blkrep n45j22ilmB_line01 n45j22ilmB_line02 1 256

> imarith n45j22ilmB.imh - n45j22ilmB_line02.hhh n45j22ilmB_clean
```

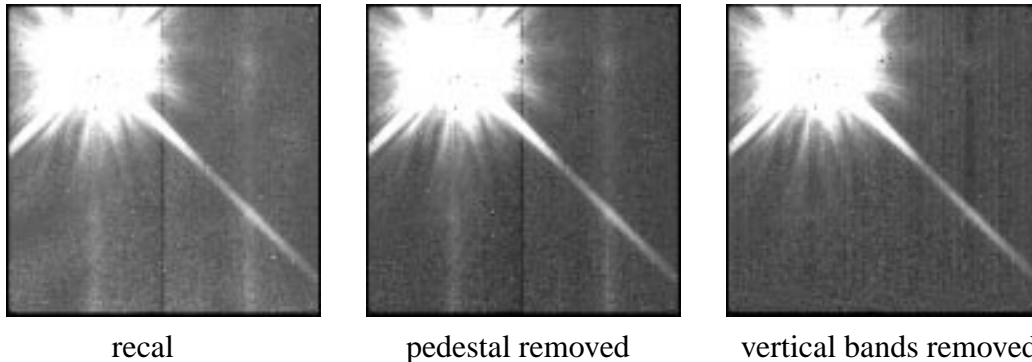


**Figure 1:** Coronagraphic image, F110W filter. Star centered in hole with image recalibrated (left), pedestal removed (middle), and vertical bands removed (right). Images displayed to the same stretch to show detail in the background.

The first 19 rows must be clean of hot and “grot” affected pixels. Otherwise, these deviant pixels will dominate the average and introduce bright or dark columns in the resulting image. If this happens, go back and use the IRAF task **fixpix** to remove the suspect pixels and re-average the first 19 rows. Figure 1 presents the same image before and after removing pedestal and the vertical bands.

The correction for removal of the vertical bands overcorrects in one quadrant, the upper right quadrant in the displayed images. This shows that the strength of the electronically reflected vertical bands depends upon the order in which the quadrants are read out. The strongest effect starts in the quadrant with the coronagraphic hole and becomes weaker going counterclockwise from quadrant to quadrant.

### ***Residual target image and electronic ghosts***

Coronagraphic observations are not dithered to image the target on different regions of the detector. There is no simple way to remove the residual image of the target due to persistence or to easily remove the electronic ghosts (“Mr. Staypuft”) of the bright pixels about the coronagraphic hole that are electronically reflected in adjacent quadrants. It is left up to observers and archival users to remove these artifacts from the images as best as possible.

### ***Coronagraphic hole location***

The coronagraphic hole location was determined from the visit 21 lamp on (flat field) and background observations, x-pos= 73.838 and y-pos = 209.477. The background and flat field images were reduced to measure the hole location in a manner similar to that performed by the Flight Software (FSW).<sup>1</sup>

## **4. Orbit-to-Orbit PSF variation (orbits 1-4)**

During each orbit of visit 22, three exposures (NUMITER = 3) were obtained with the target centered in the coronagraphic hole using the F187N and F110W filters. To achieve a meaningful comparison, the F110W filter observations were calibrated using the same reference files and reduced in a similar manner with pedestal and the vertical bands removed. The IRAF task **imcopy** was used to copy the image arrays into an image set. The task **calnicb** was used to coadd the three images. For example:

```
> copy n45j22i4m_cal.fits n45j22i4m_cl_cal.fits
> copy n45j22i5m_cal.fits n45j22i5m_cl_cal.fits
> copy n45j22i6m_cal.fits n45j22i6m_cl_cal.fits

> imcopy n45j22i4mB_clean.hhh n45j22i4m_cl_cal.fits[1][*,*]
> imcopy n45j22i5mB_clean.hhh n45j22i5m_cl_cal.fits[1][*,*]
> imcopy n45j22i6mB_clean.hhh n45j22i6m_cl_cal.fits[1][*,*]

> tedit n45j22020_clean_asn.fits
Column      1          2          3
Label  _____  _____  _____
      1  N45J22I4M_CL  EXP-TARG  yes
      2  N45J22I5M_CL  EXP-TARG  yes
      3  N45J22I6M_CL  EXP-TARG  yes
      4  N45J22020_CL  PROD-TARG  yes
```

---

1. NICMOS Instrument Science Report NICMOS-ISR-98-012.

```
> calnicb n45j22020_clean_asn.fits  
> display n45j22020_cl_mos.fits[1] 1
```

There was approximately 1 1/2 hours between each set of F110W observations. The coadded F110W filter images were subtracted (**msarith**) from each other, orbit-to-orbit. No shift of the images was performed. A section of the subtracted images, 95 x 95 pixels centered on the coronagraphic hole, are presented in Figure 2. The images were obtained with the same S/C roll and the same guide star pair was used for guiding. The images are displayed to the same stretch.

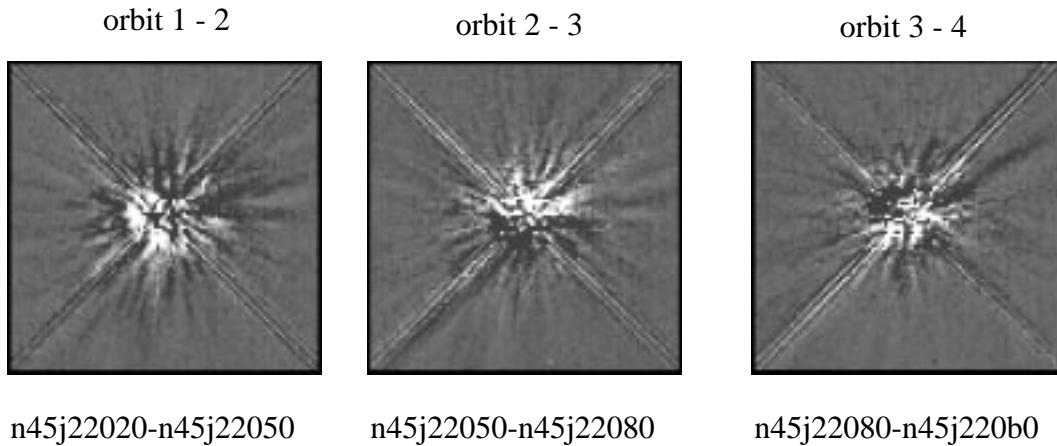


**Figure 2:** Subtraction of F110W filter images. Star imaged within the coronagraphic hole. On-board ACQ performed at start of each orbit. Enlarged images displayed, 95 x 95 pixels. Same spacecraft ORIENT used.

The coadded F110W filter images from the subsequent orbits were subtracted from the coadded F110W image from the first orbit. These images are presented in Figure 3. They are displayed in a similar manner to the images in Figure 2.

One would expect subtraction of the images to yield very small residuals. This is not the case. The remaining residual scattered light pattern indicates changes in the PSF between orbits. Possibly, a change in the position of the target relative to the hole or focus changes resulted in the different amount of residual counts.

The images displayed in Figure 3 show close alignment of the diffraction spikes. For the image “orbit 1-3”, the diffraction spike from upper left to bottom right has been completely removed, while for image “orbit 1-4”, the diffraction spike from lower left to upper right has been completely removed. This clearly shows that whatever is creating the diffraction spikes (OTA, cold mask, etc ...) has not moved.

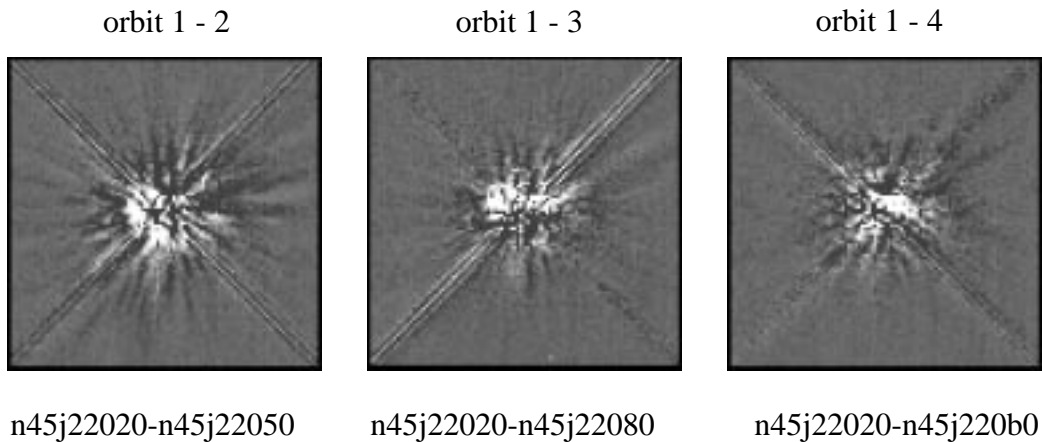


**Figure 3:** Subtraction of F110W filter images. Star imaged within the coronagraphic hole. On-board ACQ performed at start of each orbit. Enlarged images displayed, 95 x 95 pixels. Same spacecraft ORIENT used.

The light scatter about the hole indicates three relatively bright glint regions. These spectral reflections are caused by large pieces of residual material remaining on the edge of the hole following the laser ablation of the front side of the mirror. They are located on the bottom, left, and top edges of the hole in the images. See Figure 5.2 in the NICMOS Instrument Handbook, version 3.0 1999.

## 5. Rolling the Spacecraft (orbit 5)

At the start of orbit 5, the spacecraft was rolled  $36^\circ$  from the previous orbit orient position. The F110W filter observations were reduced in a similar manner to the orbits 1-4 data. Three F110W filter observations were co-added to achieve an identical S/N to the co-added orbits 1-4 observations. The co-added image was subtracted from each of the co-added orbits 1-4 observations, orbit-to-orbit. No image registration was performed. The resulting images are presented in Figure 4.

The visit 23 data were obtained with a different set of guide stars. There is an elapsed time of approximately 2 hours from the previous visit 22 orbit to the visit 23 F110W filter observations. Close inspection of the visit 23 F110W images shows these images appear to be sharper than the corresponding visit 22 images even though the bright diffraction spikes fall on the identical pixels. The focus had changed considerably during the two visits. Focus data, microns of secondary mirror motion, are presented in Table 3.

**Table 3.** Model HST focus positions day 1997.204 for the 7052 F110W data.

Visit	Orbit	observation	TIME-OBS (UT)	defocus (microns)	ORIENT
22	1	n45j22020	03:30:05	1.4	-18D TO -18D
	2	n45j22050	05:04:59	1.2	-18D TO -18D
	3	n45j22080	06:41:49	1.2	-18D TO -18D
	4	n45j220b0	08:18:36	1.1	-18D TO -18D
23	5	n45j23030	10:23:14	-1.0	+18D TO +18D

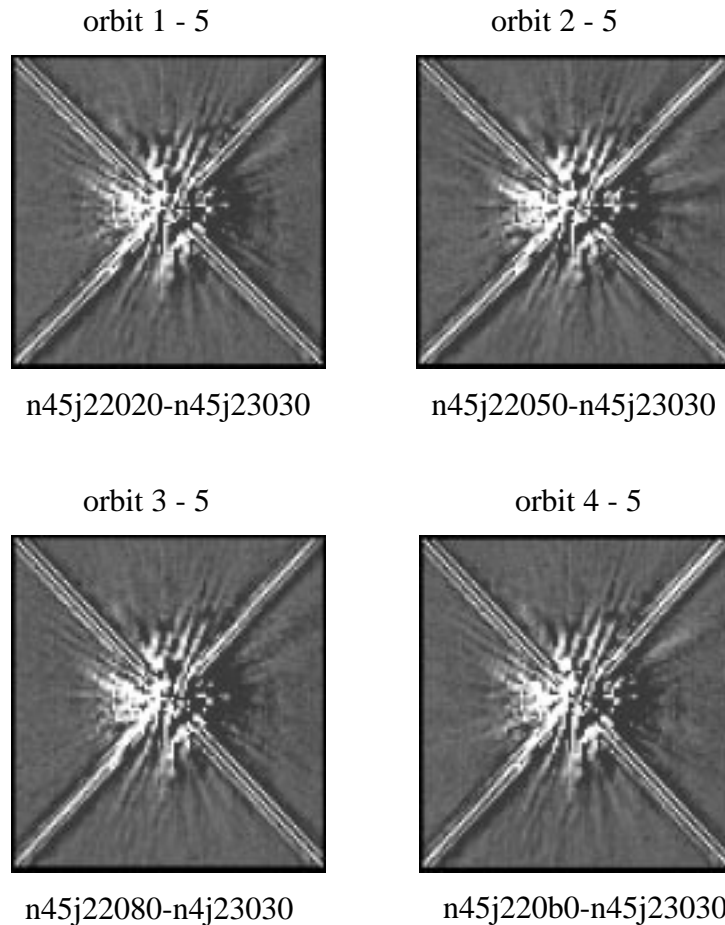


**Figure 4:** Subtraction of F110W filter images. The visit 23 coadded image (ORIENT=+18D) subtracted from the visit 22 coadded images (ORIENT=-18D). Enlarged images, 95 x 95 pixels, displayed to the same stretch.

The residuals from the subtraction of images, n45j23030 with images n45j22020, n45j22050, n45j22080, n45j220b0, evident in the displayed images in Figure 4 are due

primarily to a redistribution of light, possibly due to a combination of four processes: 1) a subpixel shift of the PSF on the array, 2) a focus change, 3) the coaddition of images by **calnicb**, and/or 4) cold mask wiggling.

Close examination of the diffraction spikes between the n45j220b0 (orbit 4) and n45j23030 (orbit 5) images shows that the diffraction spikes are imaged on essentially identical pixels. The light in the diffraction spike image is more evenly distributed over the central two rows of pixels for the orbit 4 image than for the orbit 5 image where there is more light on the upper of the central two rows of pixels. Thus, the orbit 5 coadded image appears to be sharper. Enlarged views of the diffraction spikes are displayed in Figure 5. This could be caused by a subpixel shift of the PSF on the array or possibly by movement (wiggling) of the Camera 2 cold mask at the pupil (Lyot stop) between orbits.

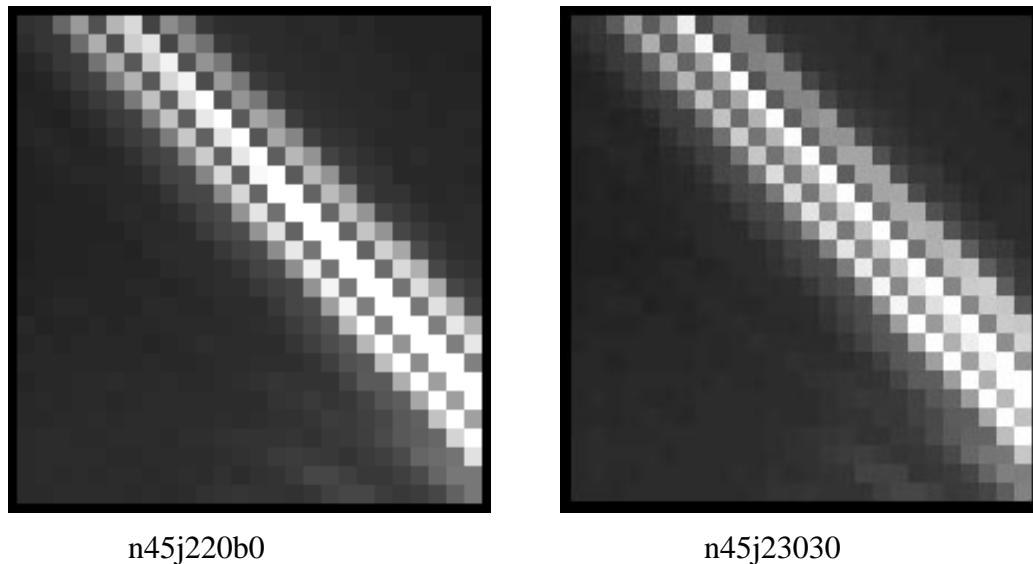


**Figure 5:** Diffraction spikes. Enlarged 25 x 25 pixel view of the upper left OTA diffraction spike from orbit 4 (n45j220b0) and orbit 5 (n45j23030) images. The telescope was rolled 36 degrees between the two images. Images displayed to the same stretch.

## 6. Individual Image Subtraction

The preceding analysis was qualitative using the coadded images. In this section, individual images are compared. The first F110W image in orbit 1 is subtracted from the second image in that orbit and from each of the first F110W images from the orbits 2, 3, and 4. These were obtained at the same pointing of the telescope. The resulting images are displayed in Figure 6.

There is a small residual remaining in the image of n45j22i4m-n45j22i5m, two images obtained back-to-back in the same orbit. The residuals are within the boundaries of the

coronagraphic hole, a region of approximately 13 x 13 pixels centered at  $x=74,y=209$ . This probably results from differences in the amount of counts removed in this region during the pedestal removal process.

The subtraction of images obtained in back-to-back orbits all show different amounts of residual counts within the region of the hole and in the regions of the diffraction spikes. These residuals indicate slight changes in the position and wings of the PSF and the light distribution within the diffraction spikes.

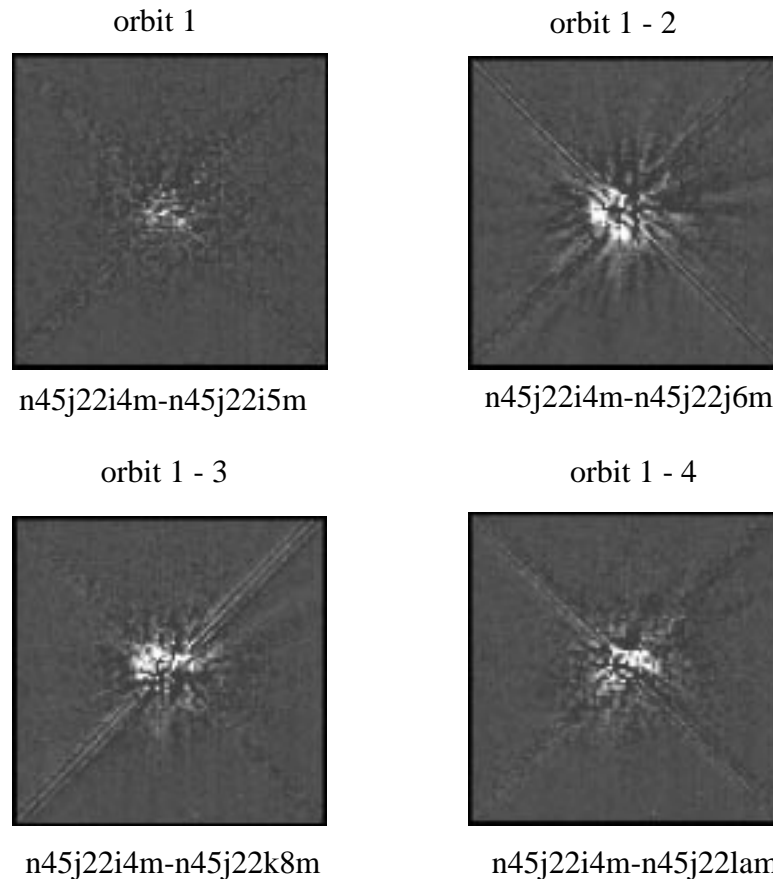


**Figure 6:** Subtraction of Individual F110W images. Images cropped to 95 x 95 pixels centered on the coronagraphic hole and displayed to the same stretch. Same spacecraft ORIENT used.

Figure 7 presents histograms of pixel counts in two images, n45j22i4m-n45j22i5m and n45j22i4m-n45j22j6m. Image regions of 13 x 13 pixels centered on the coronagraphic hole ( $x=74, y=209$ ) were set to a value of -10. The histogram of the image n45j22i4m-n45j22i5m has a narrow core, while the histogram for the image n45j22i4m-n45j22j6m has broad wings adjacent to the profile of the core. The high count values in the wings of the profile indicate the presence of residual counts from the image subtraction. These

include residual counts from light scatter about the hole as well as due to the redistribution of light within the diffraction spikes.

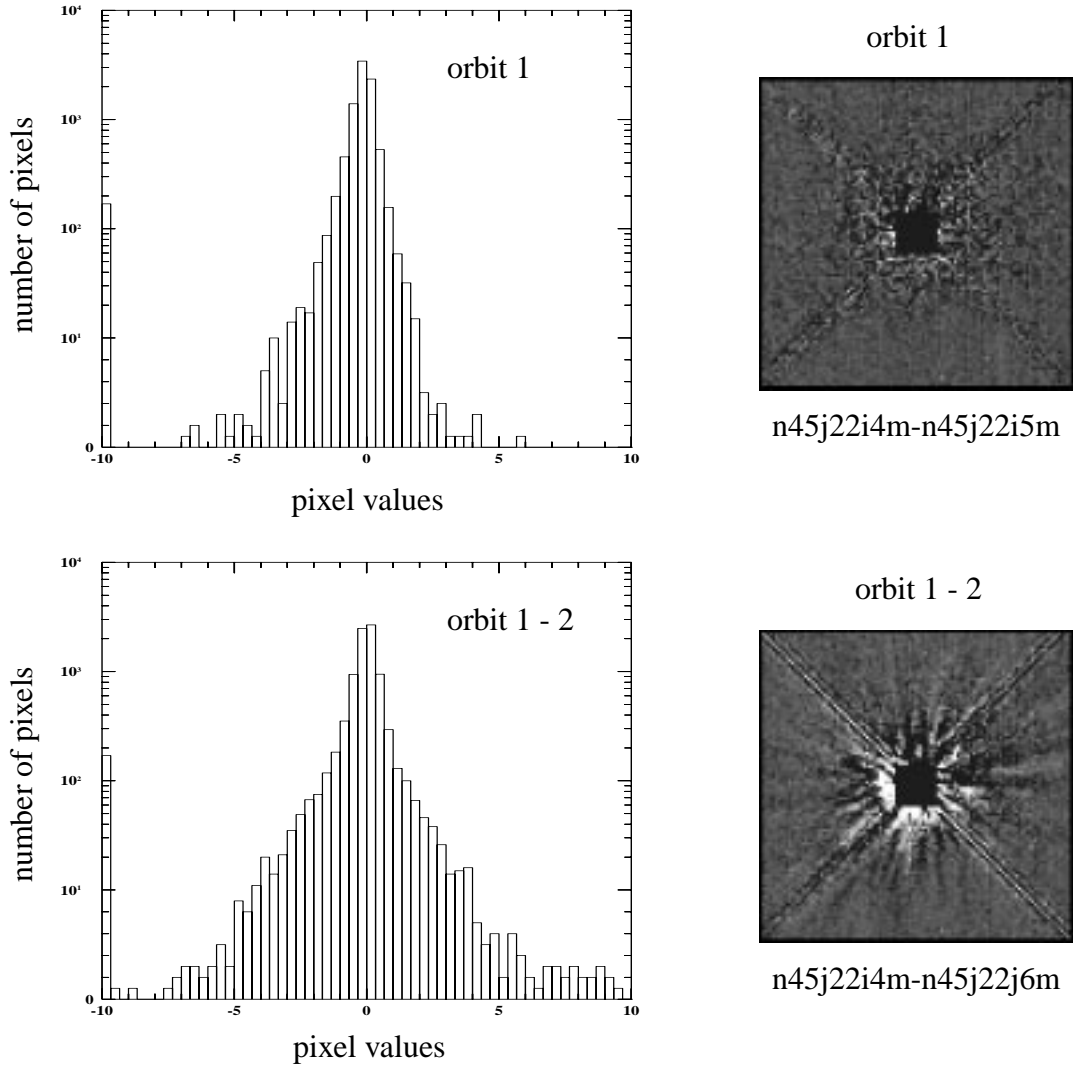


**Figure 7:** Pixel Histogram and Respective Image Area. Image area used was 95 x 95 pixels centered on the coronagraphic hole. Central 13 x 13 pixels set to a value of -10 and not used for histogram statistics. The same ORIENT was used for orbits 1 and 2. Images displayed with the same stretch.

Figure 8 presents a histogram of pixel counts and an image of an orbit 5 image subtracted from the corresponding orbit 4 image, n45j22lam-n45j23mym. The spacecraft was rolled 36 degrees between the two orbits and different guide stars acquired. Similarly, the central 13 x 13 pixels centered on the coronagraphic hole (x=74, y=209) were set to a value of -10. The histogram for this image has a narrow core with extended wings. The

residuals are abnormally high indicating a mismatch between the two images even though they were obtained in back-to-back orbits and an onboard NICMOS ACQ was performed to position the target in the aperture.

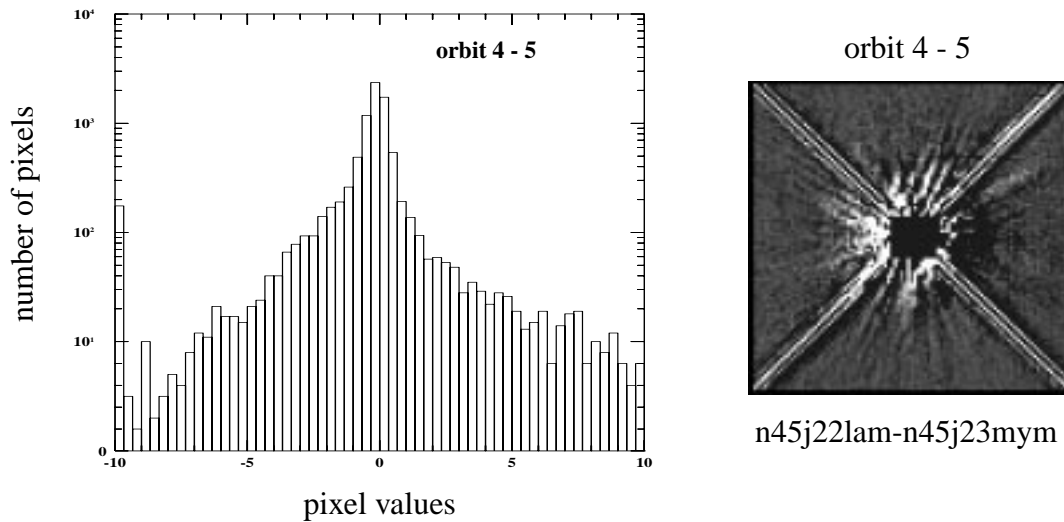


**Figure 8:** Histogram and Respective Image. The difference of two images obtained in consecutive orbits with a roll of  $36^\circ$  between orbits. A NICMOS ACQ was performed at the start of each orbit.

Image statistics (**msstat**) of the  $95 \times 95$  pixel areas centered about the hole, excluding the  $13 \times 13$  pixel area, for images discussed above are presented in Table 4. The maximum pixel deviation is found for the subtraction of images obtained in back-to-back orbits with a roll between the two orbits.

**Table 4.** Image Statistics. Image area sampled was  $95 \times 95$  pixels centered on the coronagraphic hole, excluding the central  $13 \times 13$  pixels.

Visit	Orbit	Image	mean	stddev	min	max
22	1	n45j22i4m_i5m	-0.154459	0.554815	-6.95978	5.74925
	1 - 2	n45j22i4m_j6m	0.0103292	1.23516	-9.39653	24.7445
	1 - 3	n45j22i4m_k8m	0.0144426	1.09456	-9.63676	17.2292
	1 - 4	n45j22i4m_lam	-0.0153505	0.816502	-9.67914	18.2928
23	4 - 5	n22lam_23mym	0.0971735	3.51271	-9.88331	112.375

## 7. Radial Profiles

In this section, a comparison of radial profiles, azimuthally averaged residual flux between the diffraction spikes, for single and PSF subtracted images are presented. The diffraction spikes were masked off, 8-pixels inclusive, and set to a very large negative number. This resulted in an inner radius for the radial profiles of 8-pixels ( $\sim 0.6$  arcsec). The steps required to create the mask image are presented in Appendix I.

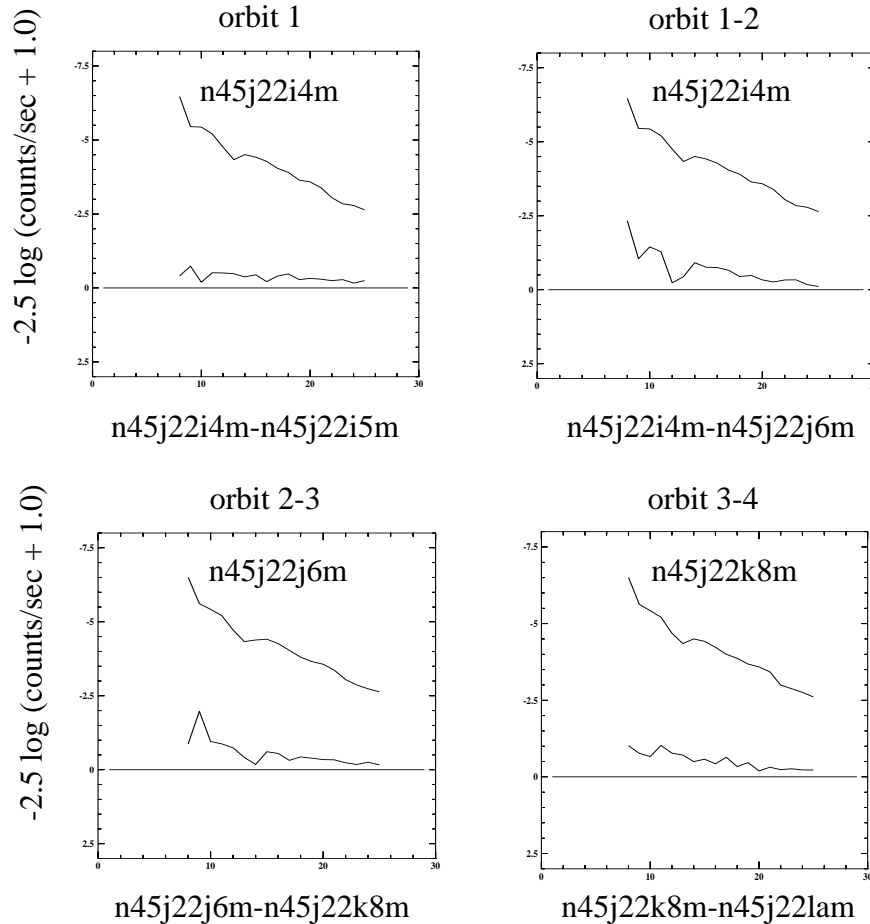


**Figure 9:** Radial profiles (pixels) centered on coronagraphic hole. Images (F110W filter) were directly subtracted with no registration of images. An ACQ was performed at the start of each orbit and the images were obtained with the same ORIENT. Upper curves, profiles of star in the hole. Lower curves, profiles after PSF subtraction.

The difference images were converted to all positive values using the IRAF task **imfunction**. An offset of 1.0 was added to each image. The IRAF apphot package task **fitsky** was used to measure the counts between the diffraction spikes. Annuli of width 1-pixel and with increasing radii of 1-pixel steps were used to measure the residual counts. The reference line in the figures represents zero counts ( $-2.5 \log (0.0 + 1.0)$ ).

Figure 9 presents the radial profiles, residual counts converted to magnitude scale, for the subtraction of images obtained in the same orbit and in consecutive orbits with the same telescope ORIENT (orbits 1-4). The images were directly subtracted with no registration of images performed.

For illustration, the radial profile of the target in the coronagraphic hole is also displayed. The smallest amount of residual counts was for the subtraction of images obtained in the same orbit with no change in ORIENT. The radial profiles from the subtraction images orbits 2-3 and 3-4 are clearly better than the subtraction image orbits 1-2. The profiles for the back-to-back orbit subtraction of images indicates the amount of settling time required for the telescope due to the change in attitude.

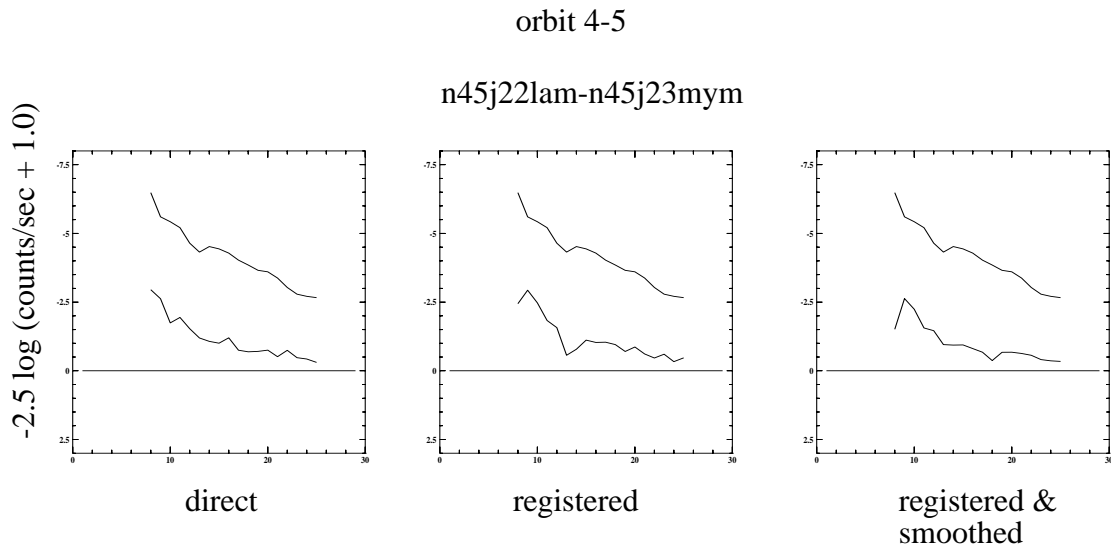


**Figure 10:** Radial profiles (pixels) centered on coronagraphic hole. Images (F110W filter) were directly subtracted, registered and subtracted, and registered, smoothed, and subtracted. An ACQ was performed at the start of each orbit and the images were obtained with different ORIENTs.

Figure 10 presents the subtraction of images obtained in back-to-back orbits with a roll of the telescope at the start of the second orbit, orbits 4-5. Three different profiles are presented; first, a profile from the direct subtraction of the images, second, a profile from the subtraction when the orbit 5 image is registered to the orbit 4 image (x-shift = -0.286, y-shift = +0.136 pixel), and third, a profile from the subtraction image for images that have been registered and smoothed with a Gaussian function (sigma = 0.8). The third profile shows the best subtraction as given by the fall off in flux at radii > 13 pixels about the line “residual background + offset” plotted on the figures. For reference, the radial profile of the star in the hole (n45j22lam) is displayed in each figure. A description for the registra-

tion of images and for smoothing of images using a Gaussian function can be found in Appendix II.

The target star was overexposed (EXPTIME=32 seconds), resulting in saturation near the coronagraphic hole. A shorter exposure would have allowed for profiles with a smaller inner radius. The amount of residual counts in the images, after subtracting a following image, depends upon how well the pedestal and the electronic ghosts (“Mr. Staypuft”) were removed from the individual images. In several of the radial profiles, large dips are evident. These excursions are due to a mismatch in the wings of the PSF, possibly caused by movement of the fore optics and/or cold mask, and focus changes.

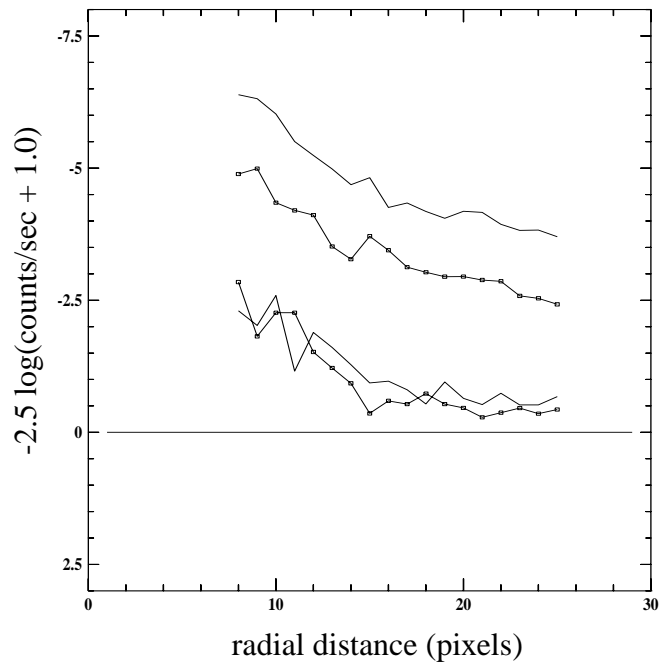
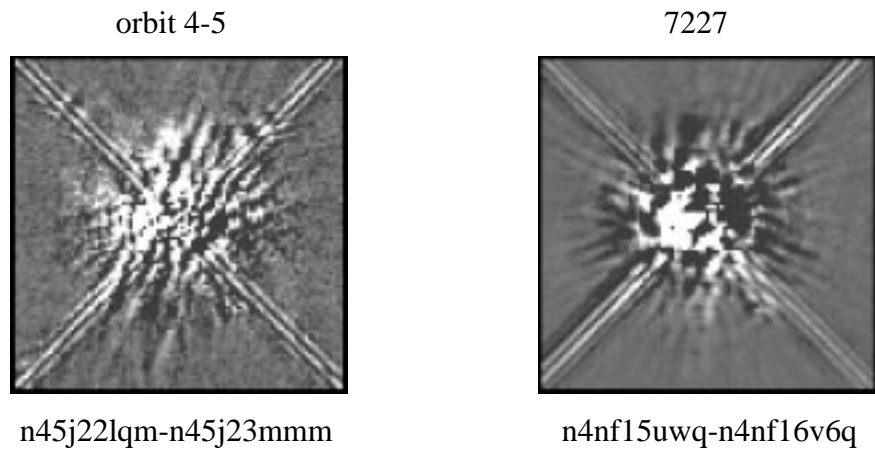
The profiles of Figure 9 indicate that good PSF subtraction for the 7052 F110W filter observations, to an inner radius of ~10 pixels (~0.75 arcsec), was achieved with the back-to-back observations with the same roll. And, the Figure 10 profiles show reasonable PSF subtraction to an inner radius of ~10 pixels for subtraction of images obtained at different spacecraft rolls in back-to-back orbits.

## **8. Back-to-Back Observations with Roll in the Same Orbit**

During Cycles 7 and 7.5, the NICMOS IDT reported exceptional results for PSF subtraction when the same target was observed twice in the same orbit with a roll of the telescope between visits (program ID: 7227). A NICMOS ACQ was performed following the roll and the hole finding routine was disabled for the second set of observations. A different set of guide stars was used for each visit. The visits were linked close in time by using the Phase II visit level requirement “AFTER”, such as AFTER 01 BY 0 TO 15 MINUTES. The links were set up so the two visits would automatically schedule in one orbit. The observations in the second half of the orbit were subtracted from the images obtained in the first half of the orbit.

In this section, a comparison of radial profiles is presented for the F160W filter SMOV 7052 and 7227 data. The data were reduced in an identical manner.

Figure 11 presents the subtraction images and the corresponding radial profiles centered on the coronagraphic hole. For the 7227 back-to-back observations n4nf15uwq and n4nf16v6q obtained in the same orbit, the image of the hole moved approximately 0.024 pixels between the time of the two observations, x-movement = -0.022, y-movement = -0.010. No flat fields were obtained at the start of each orbit for the 7052 observations and thus, the movement of the hole is unknown. The subtraction images are displayed to the same scale and stretch. The program 7052 subtraction image (orbit 4-5) exhibits high frequency residuals compared to the program 7227 subtraction image. These residuals make the 7052 observing mode less desirable for detecting faint point sources near the primary star (<1.125 arcsec).



n45j22lqm-n45j23mmm  
solid line

n4nf15uwq-n4nf16v6q  
solid line with boxes

**Figure 11:** Consecutive orbit (7052) and back-to-back same orbit (7227) subtraction images (F160W filter). Telescope rolled between pairs of observations. Images displayed to same scale and stretch. Direct subtraction with no registering of images. Radial profiles are average counts between diffraction spikes.

The Figure 11 radial profiles indicate a gain of  $\sim 0.5$  magnitude per pixel at a radial distance of 20 pixels from the hole for the program 7227 subtraction image, back-to-back observations in the same orbit, when compared with the program 7052 subtraction image

(orbit 4-5), consecutive orbit observations. The 7227 radial profile indicates good subtraction without registering the images to an inner radial distance of  $\sim 13$  pixels ( $\sim 1$  arcsec).

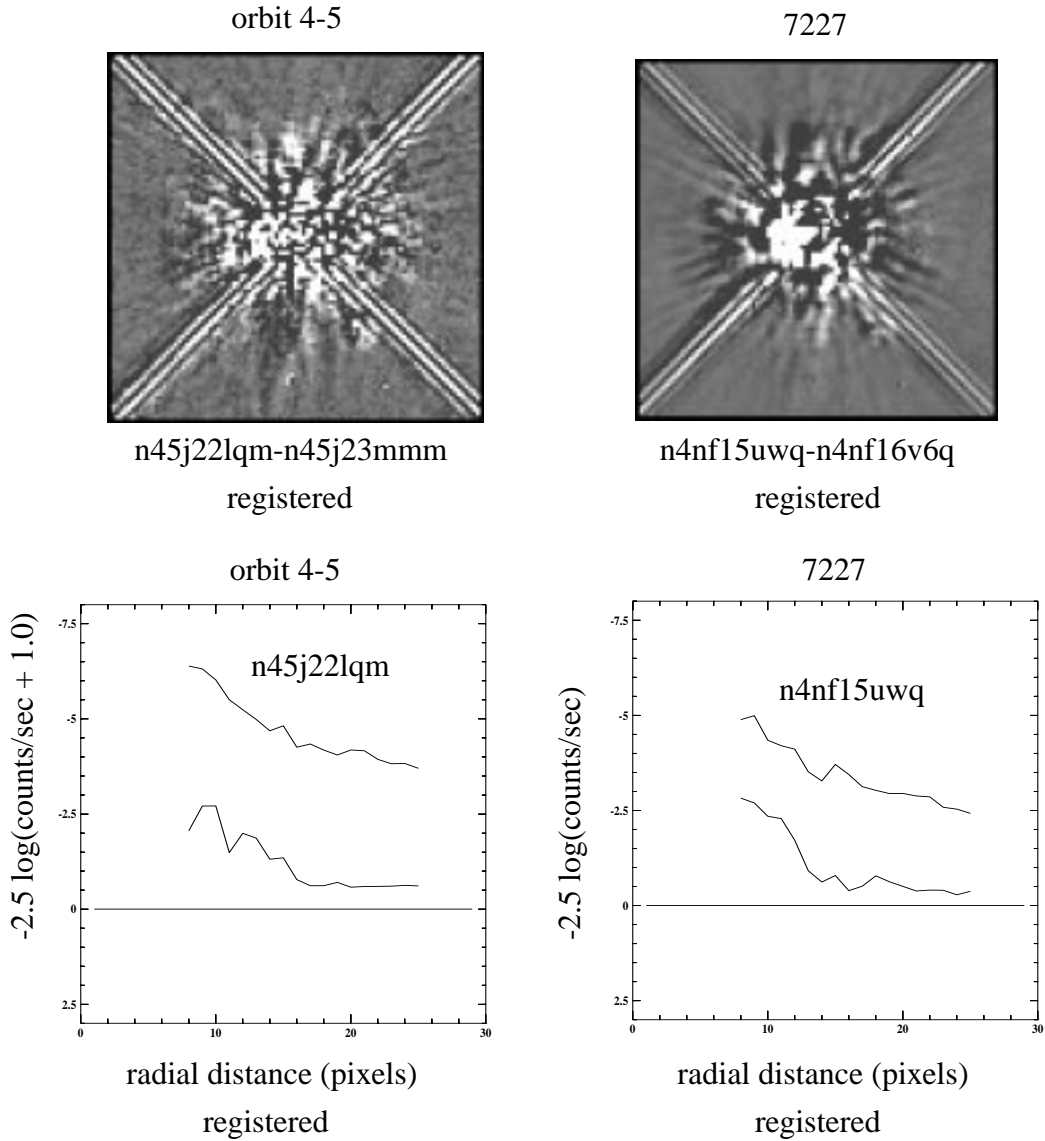


**Figure 12:** Consecutive orbit (7052) and back-to-back same orbit (7227) subtraction images (F160W). Images n45j23mmm and n4nf16v6q were shifted to match the first image and subtracted. Images displayed to same scale and stretch. Radial profiles are average counts between the diffraction spikes.

Figure 12 presents the subtraction images, programs 7052 (n45j22lqm-n45j23mmm) and 7227 (n4nf15uwq-n4nf16v6q), resulting when the second image is shifted to match the wings of the first image PSF. The IRAF task **xregister** was used to shift the n45j23mmm image (x-shift = -0.118, y-shift = +0.126) to match the n45j22lqm image.

The **xregister** task did not yield good results for image n4nf16v6q and the task **imshift** was used to shift the n4nf16v6q image (x-shift = -0.10, y-shift = 0.00) to match the n4nf15uwq image. The radial profiles presented are for the direct subtraction of the images with no smoothing performed. The light pattern for the n45j22lqm-n45j23mmm subtraction image is more symmetrical about the position of the hole, while little improvement in the light pattern was achieved by shifting to create the subtraction image n4nf15uwq-n4nf16v6q.

Two other data sets from program 7227 were investigated for this report. For completeness, the subtraction images and radial profiles are presented in Figure 13 for these two data sets.

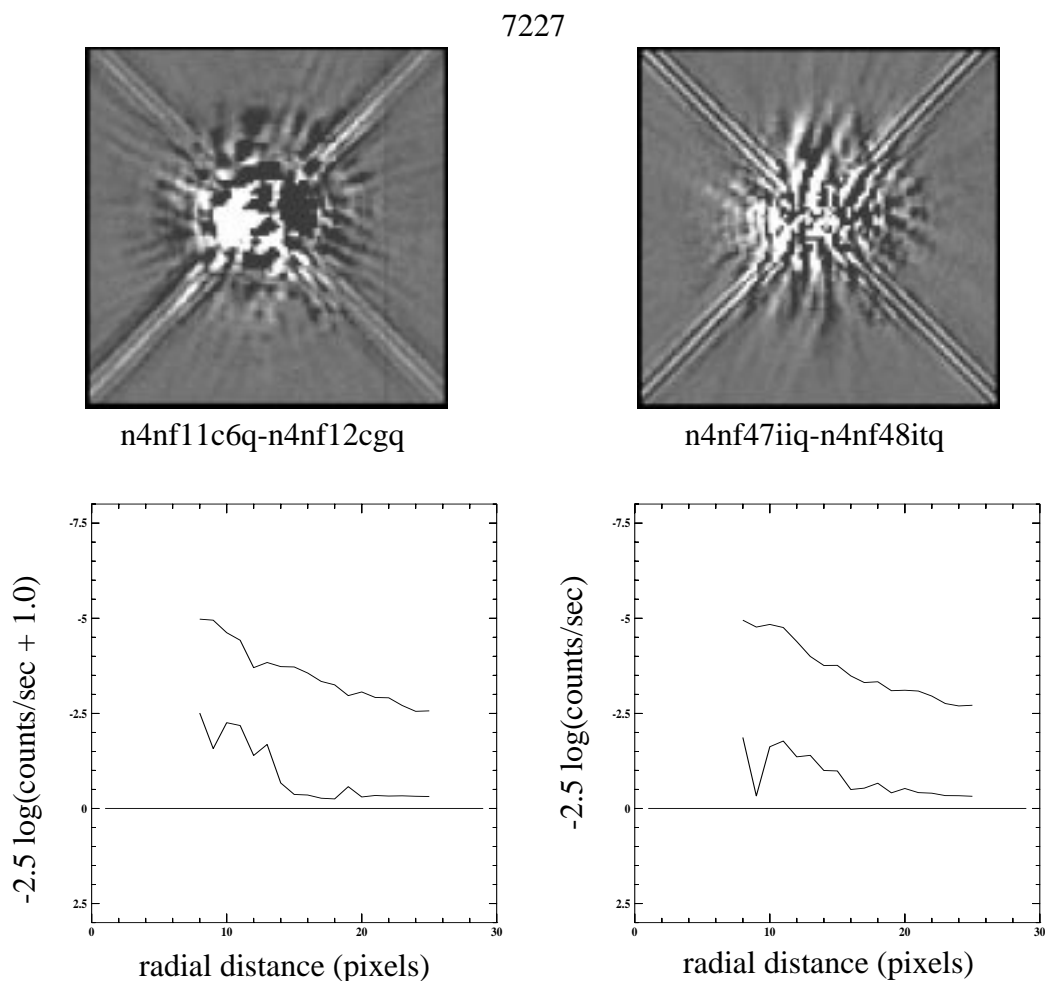


**Figure 13:** Back-to-back same orbit (7227) subtraction images (F160W). Direct subtraction of images with no registering of images. Images displayed to same scale and stretch.

The images exhibit anomalous PSF patterns, most probably due to thermal changes caused by the attitude change from the previous target to the coronagraphic target. In addi-

tion for both sets of observations, the location of the hole shifted by  $\sim 0.1$  pixel between the two back-to-back images. The temperature-based focus models for these observations are presented in Appendix III. The previous HST pointing history for the 7227 observations presented here are presented in Appendix IV.

## **9. Observational Strategy**

It must be noted that for the SMOV program 7052 F110W filter observations, the target was positioned in the center of the hole and not at a hole position to minimize the light scatter about the hole. It was determined from walking the target across the hole that decentering a point source by a small amount,  $x=-0.75$ ,  $y=-0.25$  pixels, from the center of the hole reduced the background intensity (see NICMOS IDT report “Results from SMOV 7052 NICMOS Coronagraphic Performance Verification”). Based on the 7052 results, targets in following coronagraphic programs were offset from the hole center. This offset has also been implemented in the NICMOS onboard coronagraphic acquisition (ACQ) flight software.

The following discussion is intended to show that the positional uncertainty budget for repeat observations of the same target is a function of many parameters. And, when planning coronagraphic observations, these constraints must be explored for their affect upon the observations. The observing strategy for a particular target (not the object placed in the hole) will depend upon its radial distance from the hole and the type of target, point source or extended target.

### ***Onboard acquisition***

A review of 38 Camera 2 on-board ACQs was performed and reported in NICMOS-IRS-98-012. The comparison between the flight software (FSW) and IRAF determined positions for 35 targets shows a mean difference of  $-0.008 \pm 0.030$  pixels for the x-position and a mean difference of  $-0.005 \pm 0.039$  pixels for the y-position. The IRAF determined target positions agreed quite well with the FSW determined target positions. The slight differences were most probably due to the different algorithms used to determine the centroids. Any large displacement in the position of a target in the coronagraphic hole is not due to the FSW target location algorithm. The 7052 observations executed before the FSW was updated to locate the position of the hole. Therefore, no additional FSW uncertainty was introduced due to locating the position of the hole.

### ***Filter wheel movement***

Between the visit 22 observations, the filter wheel was moved from filter F187N (position #10), to filter F110W (position #18), to filter F160W (position #19), and repeated for each orbit. The NICMOS filter wheels are repeatable to within  $\pm 0.48$  degs. The wheel diameters are not the same though, wheel 1 is the smallest and wheel 3 is the largest.

Therefore a 0.48 deg angular error is going to cause a greater displacement on Camera 3 than for the other cameras. There has been no measurable motion of the PSF in Camera 2 images due to changing the filter.

### *FGS guiding*

There were no reported problems acquiring or reacquiring the guide stars for visit 22 and 23. A check of the Fine Guidance Sensors (FGS) guide star walk downs shows the guide stars were indeed single and not binary in nature. Guide Star REacqs could possibly lock onto the wrong part of the S-curve and introduce some uncertainty in the positioning of the target. This is a very rare occurrence. But this should not have affected the positioning of the target in the coronagraphic hole as an onboard ACQ was performed following each Guide Star REacq. A check of the position of the target in the Camera 2 ACQ images for displacements reveals no problems following a GS REacq. Table 5 presents the position of the target in the NICMOS ACQ images. A synthetic dark and an on-orbit flat were used for calibration. The IRAF task **imcentroid** was used to determine the target position.

**Table 5.** 7052 target location in NICMOS ACQ images

Visit	Orbit	observation	X-pos (pixel)	Y-pos (pixel)	ACQ
22	1	n45j22i0m	172.911	107.206	GSacq
	2	n45j22j1m	157.710	124.103	GS REacq
	3	n45j22k3m	157.723	124.144	GS REacq
	4	n45j22l5m	157.664	124.063	GS REacq
23	5	n45j23m8m	160.898	107.934	GSacq

The discrepancy in the position of the target between the GSacq (orbit 1) and the GS REacq (orbit 2) is due to the difference in pointing between the initial GS acquisition and the GS re-acquisition. At the start of the first orbit, the FGS finds the guide stars and performs a center line maneuver to best locate the guide stars in the FGS FOV, called a pickle. The difference,  $\sim 1.7$  arcsec, results from the uncertainty in the guide stars and target coordinates. After the NICMOS onboard ACQ, the pointing of the telescope is well known and used in subsequent orbits to point the telescope. In essence, the uncertainty in the pointing has been removed which is reflected in the identical position of the target in the subsequent ACQ images for orbits 2, 3, and 4. This shows the repeatability of the pointing for GS REacqs is good to a few milli-arcsec (mas). And, the uncertainty of the coordinates for a new set of guide stars comes into play for the visit 23, orbit 5, GS acquisition.

### ***Orbital disturbance***

On extremely rare occurrences, after the NICMOS onboard ACQ, an orbital disturbance can cause the FGS to track a S-curve secondary null introducing a pointing change in guide stars of  $\sim 70$  mas (0.070 arcsec), which is about the size of a Camera 2 pixel. If this happens to the dominant guide star, a translation of the telescope will occur. If it happens to the subdominant guide star, the roll guide star, a roll will be introduced about the dominant guide star. The associated translation will depend upon the geometry of NIC2 and the guide stars in the focal plane. If the guide stars are diametrically across the focal plane from each other, the translation will be half,  $\sim 35$  mas. In all other cases, the induced translation will be worst.

During a recentering event, a pointing disturbance, the FGS are commanded to release the guide stars. After the event, the FGSs are command to the last known position of the guide stars and guiding is resumed. This can cause a hop to a secondary fringe and cause a translation. A review of the Observatory Management System (OMS) products show no such event occurred during the 7052 observations.

### ***NICMOS Focus and HST Breathing***

The HST focus (the focus position) is known to oscillate with a period of one HST orbit. Changes in the focus are attributed to thermal contraction/expansion of the optical telescope assembly (OTA) resulting from the telescope warm up and cool down during an orbital period.<sup>2</sup> These short term focus variations are usually referred to as “OTA breathing”, “HST breathing”, “focus breathing”, or simply “breathing”. Breathing affects all data obtained with all instruments onboard HST. Therefore, characterization of HST breathing is very important for both HST data reduction and instrument monitoring (Bely, P. 1993, SESD-93-16; Hershey, J.L. 1998, SESD-97-01, version 2.0, 06-1998).

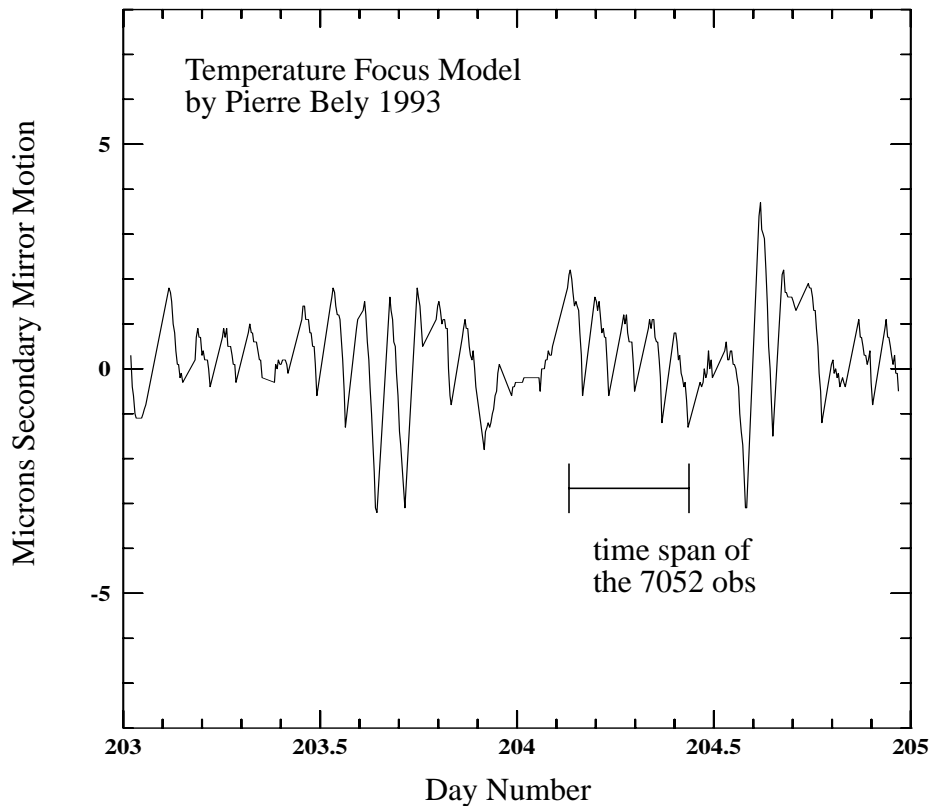
Thermally induced HST focus variations were also found to have large deviations after the telescope had slewed across a large Sun angle from a previous target to the proposed target. After a telescope slew, the telescope temperature variation exhibited the regular orbital component plus a component associated with the change in telescope attitude. The focus changes due to telescope attitude are complicated functions of Sun angle and off-nominal roll.

Figure 14 presents the temperature-based focus model during the time span of the 7052 observations. The time span for the visit 22 and 23 observations is marked on the figure and these observations executed in five back-to-back orbits. Inspection of Figure 14 indicates no large focus excursion occurred during the 7052 observations. The focus behaved in the expected manner except for the slight downward trend due to attitude.

---

2. NICMOS Instrument Science Report, NICMOS ISR-98-015

A check of the time period for the 7052 observations indicated that at the start of the first orbit observations (visit 22), there was a variation of the focus due to the change in attitude from the previous target to the 7052 target. The focus stabilized after this first set of observations and behaved in the normal orbital oscillatory manner with a slight downward trend (cooling attitude), equivalent to microns of secondary mirror motion.



**Figure 14:** Temperature-based Focus Model. Model based on four aft light-shield temperature sensor data extracted from telemetry.

## 10. Summary

The 7052 visit 22 observations were obtained at the same S/C ORIENT, but were not obtained in identical portions of the orbit. They were obtained in identical time sequence following the NICMOS onboard ACQ. No allowance was made for the shorten time for a guide star REacq, which is approximately 2 minutes less than for a full GS acquisition. The focus positions were nearly identical for the visit 22 F110W observations. Yet, residuals remain when images were subtracted from each other.

The 7052 visit 23 observations were obtained at a different S/C ORIENT than for the visit 22 observations. An onboard ACQ was performed at the start of the visit and essen-

tially positioned the target at the same location in the aperture as for the visit 22 observations. The F110W filter observations (orbit 5) executed about 2 hours following the last visit 22 F110W filter observations (orbit 4).

Figures 2 through 8 show the subtraction of NICMOS coronagraphic images obtained in back-to-back orbits. In addition, an onboard ACQ was performed at the start of each orbit. The same ORIENT was used for all visit 22 observations, while the spacecraft was rolled 36 degrees for the visit 23 observations. These images clearly show a straight subtraction of images is not sufficient for PSF subtraction. The light distribution within the PSF, the wings of the PSF, and light scatter about the hole changed sufficiently from orbit-to-orbit to yield large residuals when performing PSF subtraction. The best results close to the hole for the 7052 observations were obtained when subtracting images obtained in the same orbit.

During Cycle 7 and 7.5, the NICMOS dewar anomaly caused the coronagraphic hole to migrate to different locations on the detector. The position of the hole on the detector had been observed to move as much as  $\sim 0.25$  pixel in three orbits. The movement of the hole was found not to be linear, but rather, the hole “jitters” back and forth along an X-Y diagonal by as much as  $\pm 0.5$  pixel.<sup>3</sup> During the 5 orbit interval for the 7052 observations, the hole could have moved about a 1 pixel. The movement of the hole could explain the large residuals about the hole since the star was repositioned at the start of each orbit to the same location in the aperture.

The large diffraction spikes are caused by diffraction from the OTA assembly. They cross almost perfectly diagonally across Camera 2 images. Figure 5 shows that for the 7052 data, the diffraction spikes fall on the same pixels from orbit-to-orbit. This clearly shows that whatever is creating the diffraction spikes (OTA, cold mask, etc ...) has not moved. However, the light distribution within the diffraction spikes change from orbit-to-orbit. This could be caused by a subpixel shift of the PSF on the array and/or by movement of the Camera 2 cold mask at the pupil (Lyot stop) between orbits.

Figures 11 and 13 show that subtracting images obtained back-to-back in the same orbit with a roll of the telescope can improve the subtraction as much as 0.5 magnitudes/pixel at 12 pixels from the center of the hole. The simplest explanation for this result is that this observing strategy minimizes the cold mask movement between observations. Figure 13 shows that thermal changes due to a change in telescope attitude affect the PSF. There is no a priori way to know in advance the change in attitude of the telescope, phase and amplitude of the OTA breathing and the Sun angle and roll changes, from the previous target to the coronagraphic target until the observations are scheduled on a calendar, a Science Mission Schedule (SMS). The attitude history preceding the coronagraphic observations has a large affect upon the success or failure for PSF subtraction.

---

3. NICMOS Instrument Science Report, NICMOS-ISR-98-012.

The results reported here are complementary to those reported by Krist et al. (PASP, 110:1046-1058, 1998).

## 11. Recommendations

There are two NICMOS coronagraphic domains for point sources, those that are within the wings of the PSF of the primary source ( $\sim 15$  pixels or  $\sim 1.125$  arcsec) and those targets at larger separations ( $> 15$  pixels). Whenever the target of interest falls within the wings of the PSF, observations of the same target at a different S/C roll within the same orbit should be obtained for PSF subtraction. However, this works well when there are no large changes in telescope attitude history immediately preceding the coronagraphic observations. Otherwise, rolling the telescope within one orbit is no better than rolling the telescope in a consecutive orbit.

For targets at much larger separations from the primary source ( $> 25$  pixel,  $\sim 1.9$  arcsec), observations of the same target in consecutive orbits with a roll should be sufficient for PSF subtraction. It is important to note again that due to movement of the hole, coronagraphic observations obtained in consecutive orbits might need to be shifted before subtracting one image from the other.

Imaging close faint circumstellar disks using NICMOS coronagraphy is challenging. These structures can be as much as 10 magnitudes, or more, fainter than the primary source. The recommended observing strategy for these objects is to obtain observations with the same filter back-to-back in the same orbit with a roll of the telescope between observations, again with the same qualifiers as stated above.

To reduce the effects of thermal changes resulting from large spacecraft attitude changes, if possible, large Sun angle slews before the coronagraphic visits should be avoided. There is no guarantee, when requesting coronagraphic observations to be executed in the same orbit with a roll of the telescope, that there will be little or no change in telescope attitude. Ideally, the NICMOS coronagraphic visit could consist of two orbits with the coronagraphic science performed in the second orbit after relaxation of any thermally induced variations.

It's possible that some of the residuals observed in the subtraction of mosaic images were due to **calnicb**. See end of Section 5. If the individual images that form the mosaic require registration, some smoothing may be introduced by the bi-linear interpolation that is used by **calnicb** to shift the images. Also, even if the images are well registered, slight differences in the diffraction pattern due to movement of the coronagraphic hole may cause the **calnicb** cross-correlation routine to compute non-zero offsets between the various images. This will again lead to some smoothing, as well as misregistration.

One way around this problem is to force **calnicb** not to shift any of the images before averaging them together. This can be accomplished by adding columns of XOFFSET and

YOFFSET values to the input association table (\_asn.fits) used by calnicb and setting their data values to zero. An example of how to do this is presented in Appendix V.

## 12. Acknowledgments

The authors would like to thank Dr. Glenn Schneider (NICMOS IDT) for providing access to the NICMOS data from program 7226 and to the many discussions about rolling the spacecraft for PSF subtraction. We would also like to thank Dr. John Hershey for providing the temperature focus models and for extracting HST attitude parameters (Sun angle and off-normal roll) from the engineering telemetry that are presented in this ISR.

## 13. Appendix I - Creating a Diffraction Spike mask Image

The diffraction spike mask image was created by rotating an image by 45 deg (**rotate**), replacing the diffraction spikes by a large negative value (**imreplace**), and rotating the resulting image by -45 deg (**rotate**). The final mask image was input into the IRAF task **imcalc** and used to set the diffraction spikes to a large negative value in unrotated images. These steps are depicted in the following captured IRAF screen messages:

```
> epar rotate
PACKAGE = imgeom
TASK = rotate

input = n22lam_23mym_cl.fits[1] Input data
output = rotate_01 Output data
rotation= 45. Rotation angle in degrees
(xin = 73.838) X origin of input image in pixels
(yin = 209.477) Y origin of input image in pixels
(xout = INDEF) X origin of output image in pixels
(yout = INDEF) Y origin of output image in pixels
(ncols = INDEF) Number of columns in the output image
(nlines = INDEF) Number of lines in the output image
(interp= linear) Interpolant (nearest,linear,poly3,poly5,spline3)
(boundar= nearest) Boundary extension (nearest,constant,reflect,wrap)
(constan= 0.) Constant for constant boundary extension
(nxblock= 512) X dimension of working block size in pixels
(nyblock= 512) Y dimension of working block size in pixels
(verbose= yes) Print messages about the progress of the task ?
(mode = ql)
:go
Transforming image n22lam_23mym_cl.fits[1] to image rotate_01
xshift: -107.89 yshift: 209.48 xmag: 1.00 ymag: 1.00 xrot: 45.00 yrot: 45.00

> imreplace rotate_01.hhh[1:256,125:132] -10000
> imreplace rotate_01.hhh[125:132,1:256] -10000

> epar rotate
```

```

PACKAGE = imgeom
TASK = rotate

input = rotate_01.hhh Input data
output = rotate_02 Output data
rotation= -45. Rotation angle in degrees
(xin = 128.) X origin of input image in pixels
(yin = 128.) Y origin of input image in pixels
(xout = 73.838) X origin of output image in pixels
(yout = 209.477) Y origin of output image in pixels
(ncols = INDEF) Number of columns in the output image
(nlines = INDEF) Number of lines in the output image
(interpo= linear) Interpolant (nearest,lin-
ear,poly3,poly5,spline3)
(boundar= nearest) Boundary extension (nearest,con-
stant,reflect,wra
(constan= 0.) Constant for constant boundary extension
(nxblock= 512) X dimension of working block size in pix-
els
(nyblock= 512) Y dimension of working block size in pix-
els
(verbose= yes) Print messages about the progress of the
task ?
(mode = ql)
:go

> epar imcal
PACKAGE = imgtools
TASK = imcalc

input = rotate_02.hhh,n45j22i4m_cal.fits[1] input image names
output = t45j22i4m_cal output image name
equals = if im1 .le. -9000 then -10000 else im2 command string
(pixeltype= real) output pixel type
(nullval= 0.) value to substitute for undefined expres-
sion
(verbose= yes) print percent done?
(mode = al)
:go

```

## 14. Appendix II - PSF Subtraction

The subtraction of images obtained in back-to-back orbits indicates the need for sub-pixel shifting or possibly the images should be convolved with a Gaussian function to match the observed PSF before subtraction. The following discussion applies both reduction techniques to two of the 7052 F110W filter images, one from orbit 4 and the other from orbit 5, in which the S/C was rolled 36 degrees.

### *Subpixel Shifting*

For those 7052 observations with the target in the hole, the light distribution about the hole should be essentially identical. This should also be the case for those coronagraphic observations using an onboard acquisition that executed after 1998 June 28. Image registration was performed using the IRAF task **xregister**. A 95 x 95 pixel area about the hole was selected as the area to be used for cross-correlation. For example:

```
> epar xregister
PACKAGE = immatch
TASK = xregister

input = n45j23mym_cl_cal.fits[1]  Input images to be registered
referenc= n45j22lam_cl_cal.fits[1]  Input reference images
regions = [27:121,162:256]  Reference image regions used for regis-
tration
shifts = xreg_shift.da  Input/output shifts database file
(output = xreg_shift01)  Output registered images
(databas= yes)  Write the shifts file in database format ?
(append = yes)  Open shifts database for writing in append
mode
(records= )  List of shifts database records
(coords = )  Input coordinate files defining the ini-
tial shift
(xlag = 0)  Initial shift in x
(ylag = 0)  Initial shift in y
(dxlag = 0)  Incremental shift in x
(dylag = 0)  Incremental shift in y
(backgro= none)  Background fitting function
(border = INDEF)  Width of border for background fitting
(lorejec= INDEF)  Low side k-sigma rejection factor
(hirejec= INDEF)  High side k-sigma rejection factor
(apodize= 0.)  Fraction of endpoints to apodize
(filter = none)  Spatially filter the data
(correla= discrete)  Cross-correlation function
(xwindow= 11)  Width of correlation window in x
(ywindow= 11)  Width of correlation window in y
(funcntio= centroid)  Correlation peak centering function
(xcbox = 5)  X box width for centering correlation peak
(ycbox = 5)  Y box width for fitting correlation peak
(interp_= linear)  Interpolant (nearest,linear,poly3,poly5,
spline3)
(boundar= nearest)  Boundary (constant,nearest,reflect,wrap)
(constan= 0.)  Constant for constant boundary extension
(interac= no)  Interactive mode ?
(verbose= yes)  Verbose mode ?
(graphic= stdgraph)  The standard graphics device
(display= stdimage)  The standard image display device
(gcomman= )  The graphics cursor
(icomman= )  The image display cursor
```

```
(mode = q1)
:go
Average shift from n45j23mym_cl_cal.fits[1] to n45j22lam_cl_cal.fits is
-0.2868552 0.1359315 pixels
Shifting image n45j23mym_cl_cal.fits[1] to image xreg_shift01 ...
```

The **xregister** task determined that a shift of  $x = -0.286$ ,  $y = 0.136$  pixels was required to register the orbit 5 image n45j23mym with the orbit 4 image n45j22lam and applied this shift to the orbit 5 image. Note that the shift along the y-axis is about 1/8 pixel, while the shift along the x-axis is about 1/4 pixel. Since NICMOS Camera 2 is diffraction limited, 2-pixels are the size of the Airy disk. A linear function was selected for the subpixel interpolation. The Nyquist criterion states that the sampling must be equal to or smaller than 1/2 the finest detail within an image to resolve a point source. Camera 2 satisfies this criterion.

The shifted orbit 5 image was subtracted from the orbit 4 image. The IRAF task **imarith** was used to perform the subtraction. For example:

```
> imarith n45j22lam_cl_cal.fits[1] - xreg_shift01.hhh dif_xreg_shift01
> display n22lam_23mym_cl_cal.fits[1][27:121,162:256] 1 z1=-1 z2=20 zr- zs-
> display dif_xreg_shift01.hhh[27:121,162:256] 2 z1=-1 z2=20 zr- zs-
```

Figure 15 displays the subtraction of the two images, the subtraction using the unshifted orbit 5 image (unregistered) and the subtraction using the shifted orbit 5 image (registered). The images are displayed to the same stretch. The subtraction using the shifted orbit 5 image exhibits a more symmetrical residual light pattern about the hole. The bright residual streak directly below the position of the hole is probably due to uncorrected removal of the vertical band (“Mr. Staypuft”) in this quadrant.

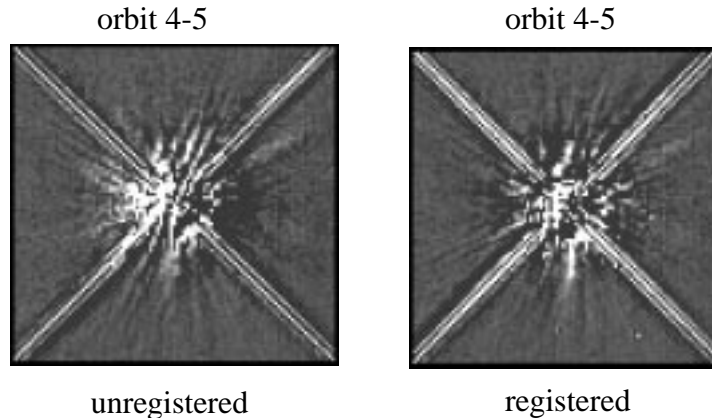


**Figure 15:** PSF Subtraction. F110W filter images obtained in back-to-back orbits with a roll of the S/C between orbits. Direct subtraction of images (left) and a subtraction with the second image shifted to match the first image (right).

Whenever there is interpolation, there will be some smoothing of the data. The subtraction of the blurred image from the unblurred image has the effect of edge enhancement.

### *Gaussian Convolution*

Figure 5 shows that for the 7052 data, the diffraction spikes fall on the same pixels from orbit-to-orbit, and that the light distribution within the diffraction spikes change from orbit-to-orbit. Registering the images to a common point does not correct for the change in the distribution of light. In this section, we discuss convolving the images with a Gaussian function to identically smooth both images.

The Gaussian function is a bell shaped probability curve defined by its sigma,  $\sigma$ , or standard deviation. Here sigma plays the role of an adjustable smoothing parameter. The degree of smoothing will be controlled by adjusting sigma. The larger sigma becomes, the higher the degree of smoothing. Convolution of the images with a Gaussian function will smooth, or blur, the edges. The averaging has the effect of suppressing the high-frequency variations in the images.

Due to the small Camera 2 field of view (FOV), there are no background stars in the images that can be used to measure the PSF. The IRAF task `fitpsf` was used to measure the sigma of the target image in the ACQ images. Though the ACQs executed at the start of each orbit, they were obtained at a slightly different focus than for the coronagraphic data. The model focus positions for the ACQ and F110W images are presented in Table 6.

**Table 6.** Model HST focus positions day 1997.204 for the 7052 F110W data.

Visit	Orbit	observation	TIME-OBS (UT)	defocus (microns)	OBSMODE
22	1	n45j22i0m	03:19:45	2.0	ACQ, F187M
	1	n45j22020	03:30:05	1.4	MULTIACCUM
	2	n45j22j1m	04:54:39	1.3	ACQ, F187N
	2	n45j22050	05:04:59	1.2	MULTIACCUM
	3	n45j22k3m	06:31:29	1.2	ACQ, F187N
	3	n45j22080	06:41:49	1.2	MULTIACCUM
	4	n45j22l5m	08:08:16	1.0	ACQ, F187N
	4	n45j220b0	08:18:36	1.1	MULTIACCUM
23	5	n45j23m8m	09:46:59	0.6	ACQ, F187N
	5	n45j23030	10:23:14	-1.0	MULTIACCUM

The measured sigmas for the target in the ACQ images (F187N filter) were identical,  $\sigma = 0.88 \pm 0.01$ . A star imaged with the F187N filter has a narrower PSF than when imaged with the F110W filter. However, the measured sigma is a good convolution starting point.

The IRAF task **gauss** was used to smooth the images. The resulting images for two different sigmas,  $\sigma = 0.4$  and  $\sigma = 0.8$ , are presented in Figure 16. For example:

```
> epar gauss
PACKAGE = imfilter
TASK = gauss

input = n45j22lam_cl_cal.fits[1] Input images to be fit
output = g45j22lam_cl_4 Output images
sigma = 0.4 Sigma of Gaussian along major axis of
ellipse
(ratio = 1.) Ratio of sigma in y to x
(theta = 0.) Position angle of ellipse
(nsigma = 4.) Extent of Gaussian kernel in sigma
(bilinea= yes) Use bilinear approximation to Gaussian
kernel
(boundar= nearest) Boundary (constant,nearest,reflect,wrap)
(constan= 0.) Constant for boundary extension
(mode = ql)
:go
```

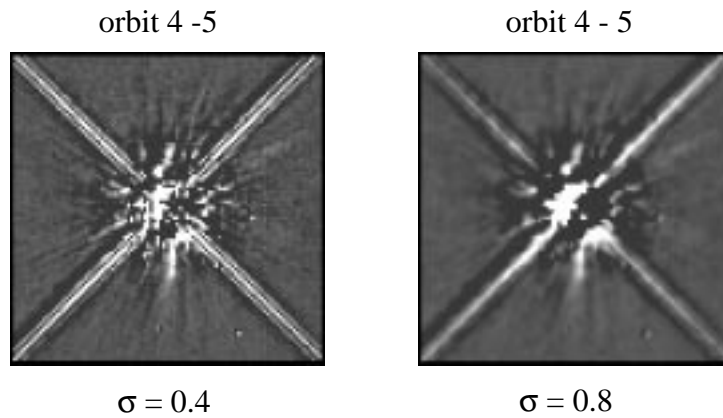


**Figure 16:** PSF Subtraction. F110W filter images obtained in back-to-back orbits with a roll of the S/C between orbits. Images convolved with a Gaussian function,  $\sigma = 0.4$  (left) and  $\sigma = 0.8$  (right) and subtracted.

The choice of 0.4 for sigma results in an image that is slightly improved from the images displayed in Figure 10. Possibly, this choice for sigma is undersmoothing the data. The choice of 0.8 for sigma results in a smoothed image that more matches the low frequency components. The proper degree of desired smoothing is left up to the user to decide.

## 15. Appendix III - Temperature Focus Models for 7227 Observations

A check of the focus model for the time periods of the 7227 observations, that were reviewed for this report, indicates the attitude change of the spacecraft from the previous target to the coronagraphic target resulted in large variations in the focus. Figures 17 and 18 presents the temperature-based focus models during the time span of the 7227 observations. The time spans for the observations are marked on the plots and the plot scales are identical to Figure 14.

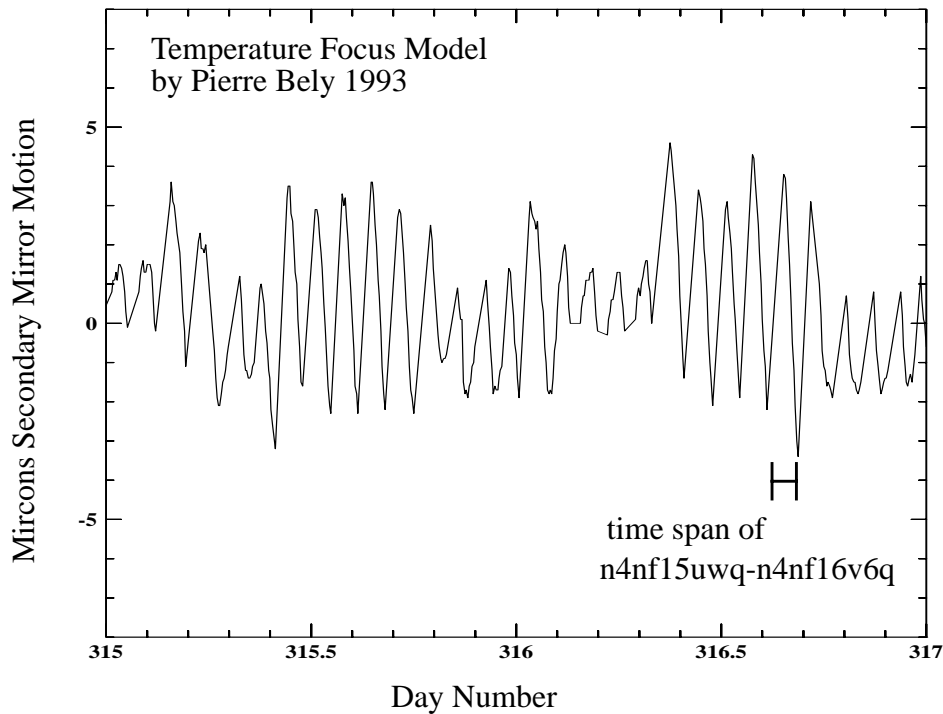


**Figure 17:** Temperature-based Focus Model for 7227 observations n4nf15uwq-n4nf16v6q. Model based on four aft light-shield temperature sensor data from telemetry.

The Bely focus model indicates, for the data set n4nf15uwq-n4nf16v6q, that the focus had reached equilibrium with a constant orbital amplitude before the start of the observations. The data set n4nf15uwq-n4nf16v6q yielded the best PSF subtraction results for observations obtained back-to-back in the same orbit with a roll of the spacecraft. The focus behaved in the expected manner for these observations

For the data sets n4nf11c6q-n4nf12cgq and n4nf47iiq-n4nf48itq, Figure 18, the temperature focus model predicts an abrupt change in the focus. Since these are single orbit visits, the telescope attitude changed before and after the coronagraphic observations. The induced HST focus variations have large deviations from the normal orbital amplitude before and after the telescope slewed to the coronagraphic target. Following the coronagraphic observations, the telescope focus variation exhibited the regular orbital breathing

pattern. The model indicates that the focus was near the average, but never the less, the PSFs are atypical.

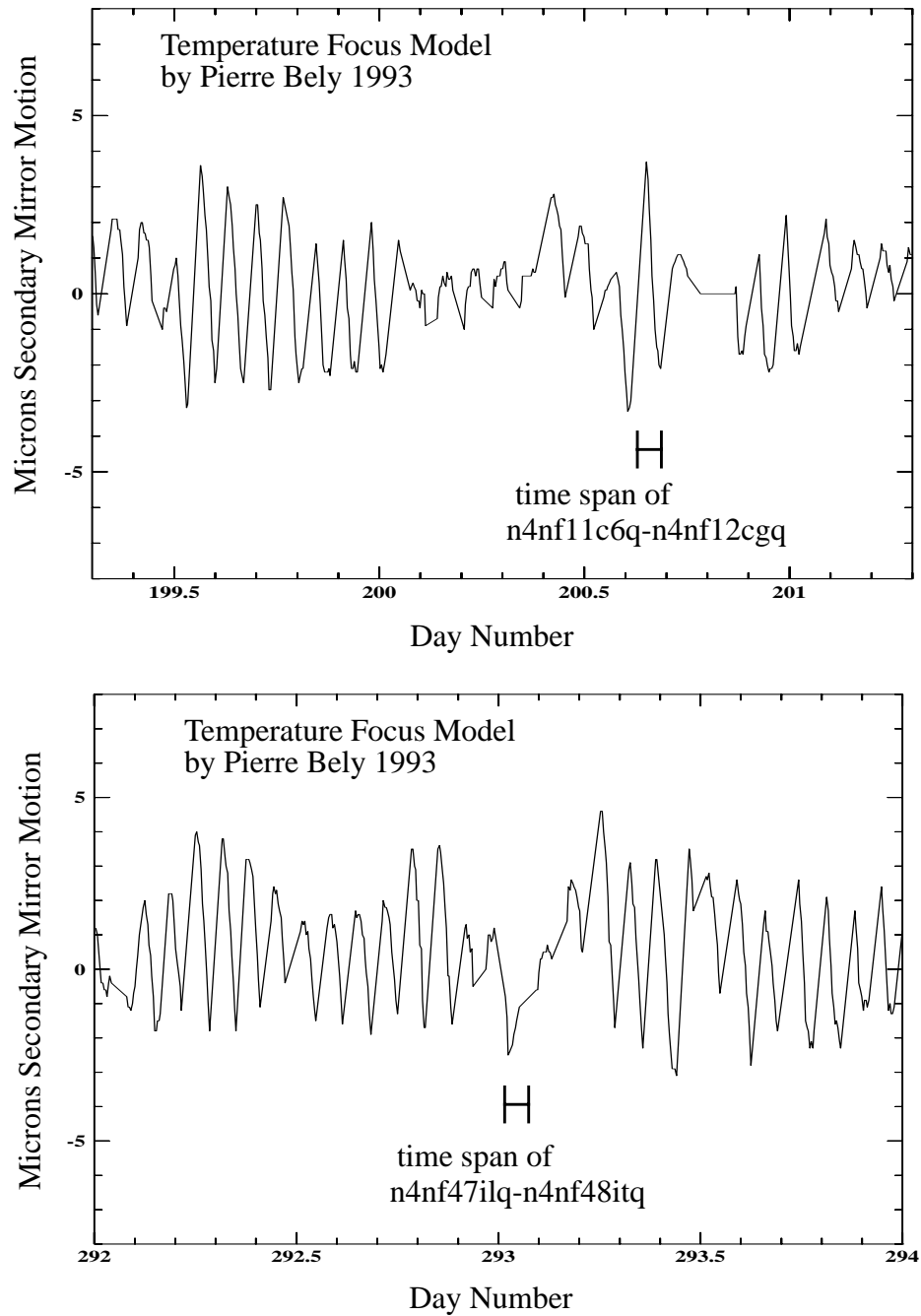


**Figure 18:** Temperature-based Focus Model for 7227 observation. Model based on four aft light-shield temperature sensor data from telemetry.

## 16. Appendix IV - HST Attitude Parameters

The following review is in reference to detecting faint point sources within the wings of the PSF for separations of 10-15 pixels (0.750-1.125 arcsec) from the center of the hole. A comprehensive rating for PSF subtraction is quite difficult, mainly due to the subjective nature of the process. The NICMOS IDT base their evaluations for the success of the subtraction on the amount of remaining residual counts in the images that are above the photon noise for different radii from the hole. In this section, only a subjective rating (good, fair, poor) is performed. The PSF subtraction was judged “good” if the subtraction removed the wings of the PSF close to the hole, “fair” if some residuals remained, and “poor” when large residuals remained. In addition, this performance rating is compared to the pointing of the telescope before and during the coronagraphic observations.

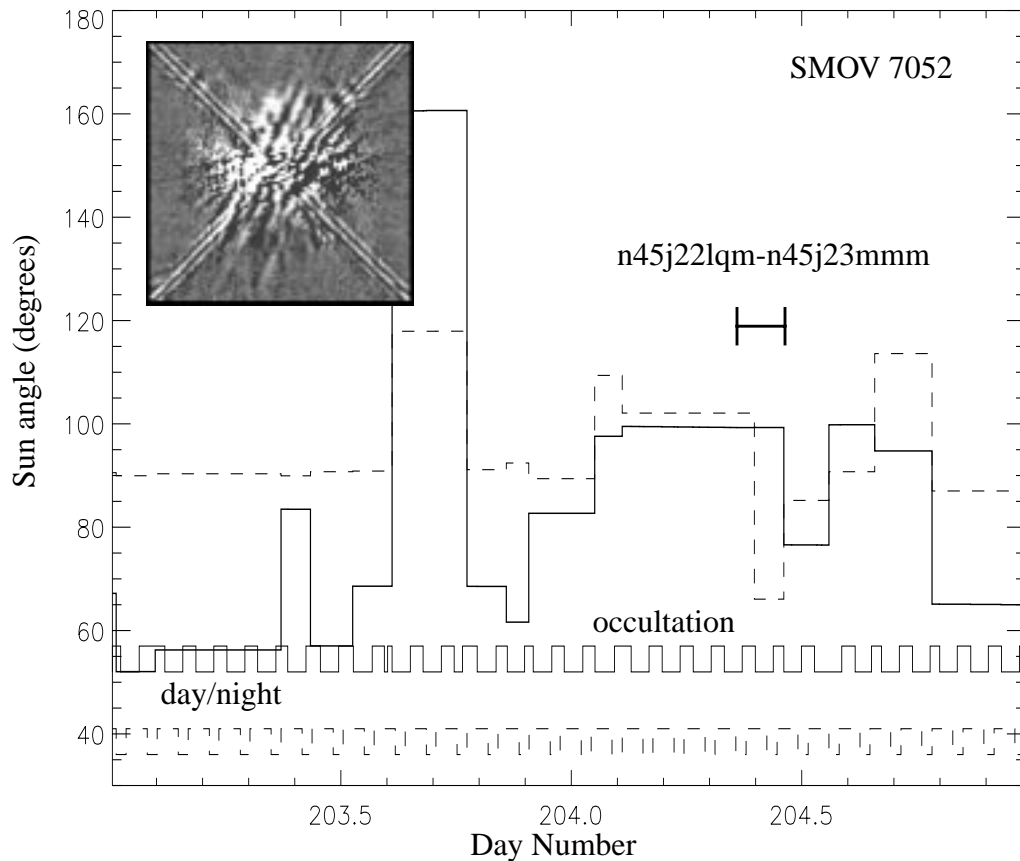


**Figure 19:** HST Attitude History for SMOV 7052.

Figure 19 displays the HST attitude history for the SMOV 7052 coronagraphic observations. The subtraction image n45j22lqm-n45j23mmm is displayed and is judged “fair”. The attitude parameters (Sun angle and off-normal roll) were extracted from the engineering telemetry and plotted versus day number. At the bottom of the figure are plotted the

orbital day/night transitions (dashed line) and above this are plotted the entry and exit of Earth occultations (solid line). There was an  $\sim 15^\circ$  change in the Sun angle at the start of the observations. In this and following figures, the Sun angle is represented by a dark “thick line” and the off-normal roll plus  $90^\circ$  plotted (to move the line above the bottom of the figures) as a “dashed line”. The time span of the coronagraphic observations is marked by the large “H-like” spacing bar.

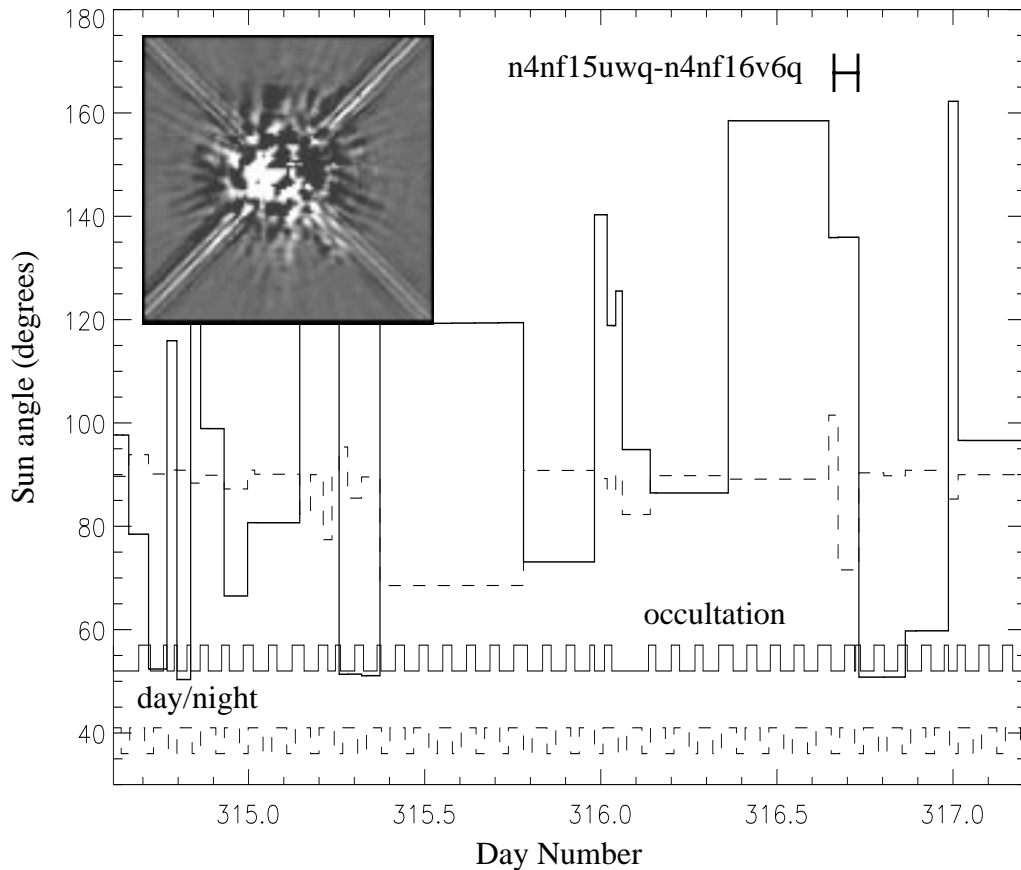


**Figure 20:** HST Attitude History for n4nf15uwq-n4nf16v6q (good).

A “good” PSF subtraction is represented by the 7227 subtraction image n4nf15uwq-n4nf16v6q, Figure 20. The telescope was at a Sun angle of  $160^\circ$  for five orbits before slewing to the coronagraphic target at a Sun angle of  $135^\circ$ . The off normal roll was  $\pm 12^\circ$  for the coronagraphic observations. The temperature based focus models (Figure 17) indicate that the focus behaved in the normal orbital oscillatory manner with a slight downward trend (cooling attitude) similar to the 7052 focus data presented in Figure 14.

A “fair” PSF subtraction is represented by the 7227 subtraction image n4nf47iiq-n4nf48itq, Figure 21. These observations were preceded by a coronagraphic observation

for program 7233. The telescope was at a Sun angle of  $145^\circ$  for five orbits and followed in sequence by two orbits at  $165^\circ$ , one orbit at  $65^\circ$ , two orbits at  $92^\circ$  (for the 7233 observations), and one orbit for the 7227 coronagraphic observation at a Sun angle of  $90^\circ$ . The off normal roll was approximately  $\pm 15^\circ$ . Though of small amplitude, the temperature based focus models (Figure 18) indicate an abrupt change in the focus oscillatory pattern.

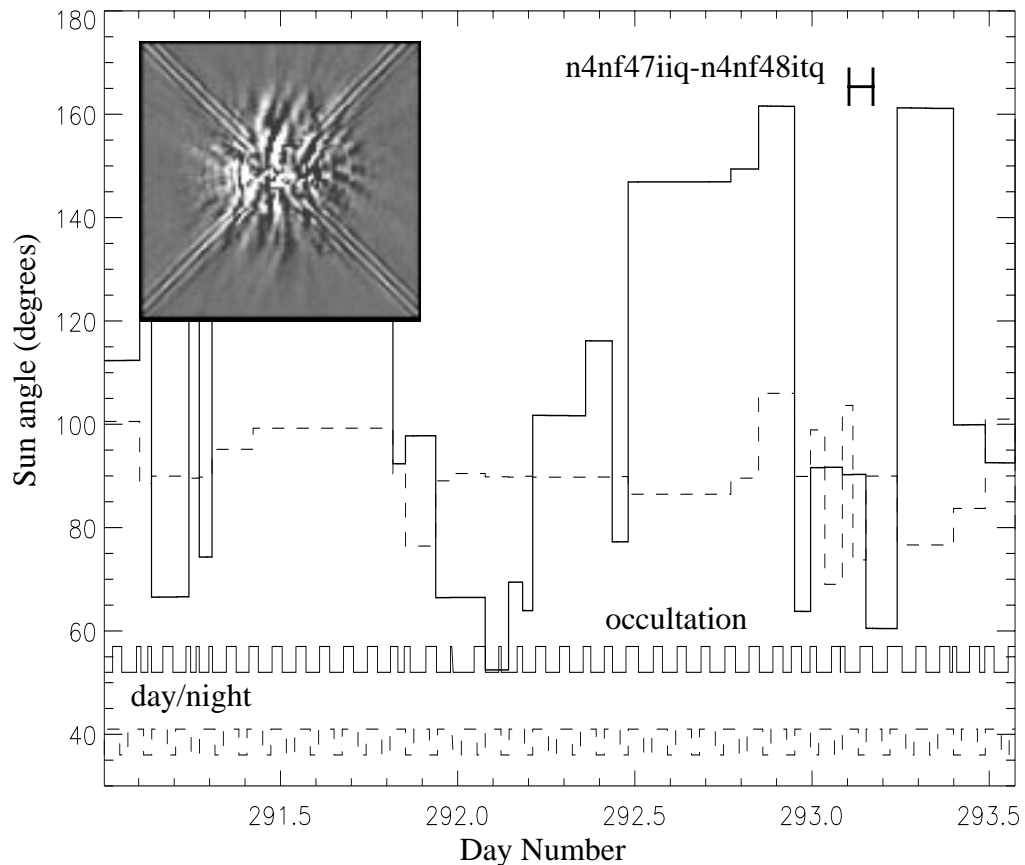


**Figure 21:** HST Attitude History for n4nf47iiq-n4nf48itq (fair).

An example of a “good-fair” subtraction is the subtraction image n4nf13lcq-n4nf14lmq (program ID: 7227), Figure 22. The Sun angle was  $115^\circ$  for four orbits and changed by  $+30^\circ$  to  $145^\circ$  for the 7227 coronagraphic observations. The Sun angle changed from a warm to a warmer angle. The off-normal roll was  $+20^\circ/-10^\circ$ . The temperature based focus models indicate that the focus behaved in the normal orbital oscillatory manner with a slight downward trend (cooling attitude).

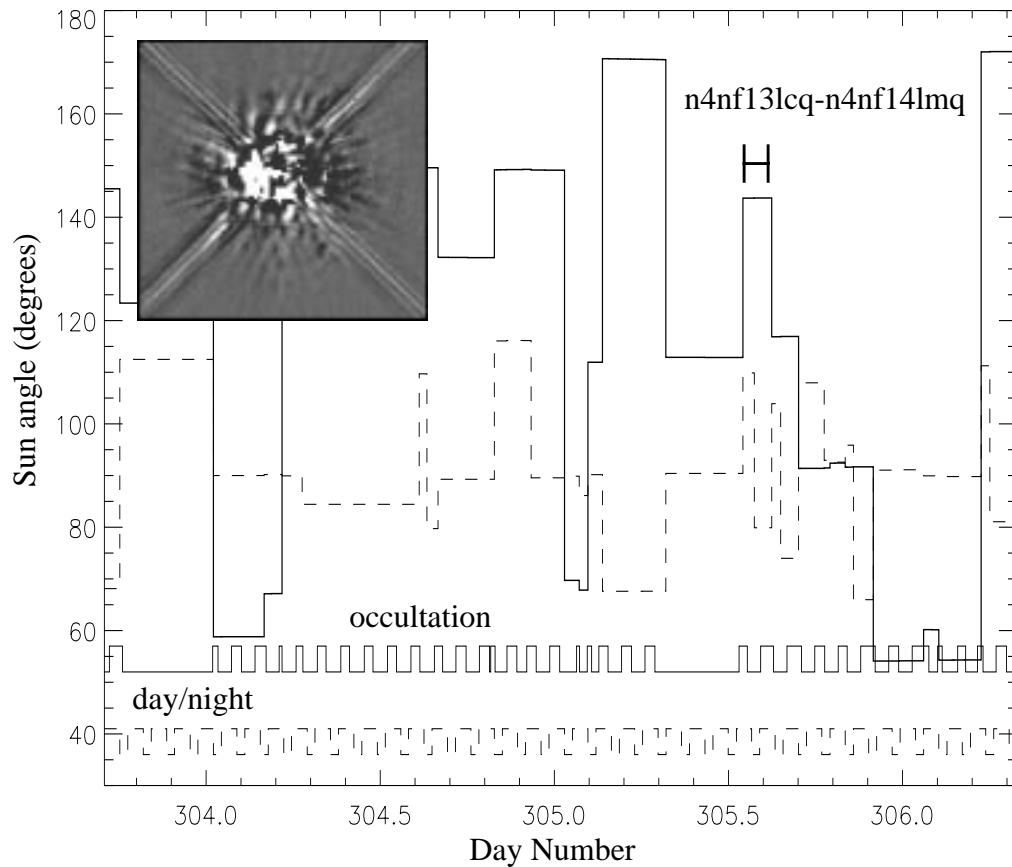


**Figure 22:** HST Attitude History for n4nf13lcq-n4nf14lmq (good-fair).

An example of a “poor” subtraction is the subtraction image imageA-imageB, Figure 23. At the request of the observing team, the identification of the program, target, and filter used for the observations are not reported. The Sun angle was at  $145^{\circ}$  for the preceding coronagraphic observations, followed by a change of  $-25^{\circ}$  from a warm to cooler Sun angle. The PSF was changing during the first set of coronagraphic observations (imageA), most probably due to the thermal change to the telescope resulting from the change in Sun angle. The off-normal roll was  $\pm 15^{\circ}$ . The temperature based focus models indicate that the focus behaved in the normal orbital oscillatory manner with a slight downward trend (cooling attitude).

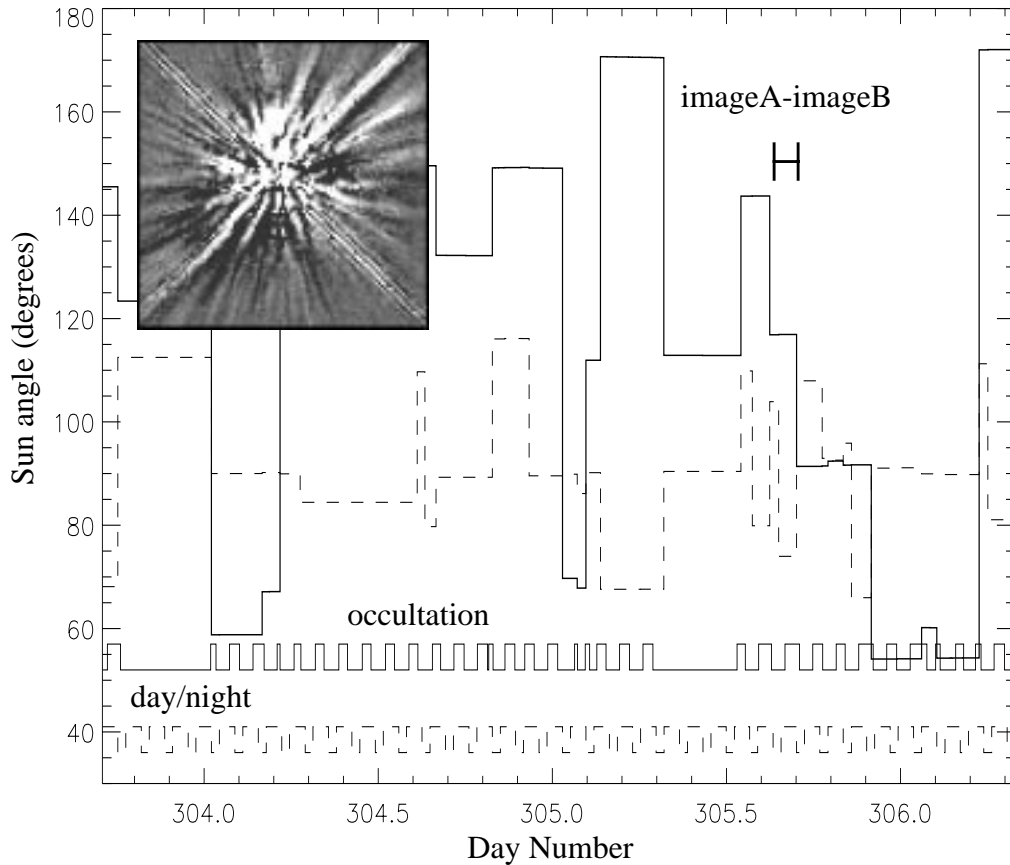


**Figure 23:** HST Attitude History for imageA-imageB (poor).

A review of the HST pointing histories and the PSF subtraction images presented in this section indicates that the temperature based focus models do not track the NICMOS PSF variations resulting from changes in Sun angle. There does appear to be a trend: one can slew farther from a cool to warmer Sun angle before the PSF is adversely affected than when slewing from a warmer to cooler Sun angle. The qualifiers are the starting point for the previous Sun angle and the amount of time the telescope was at that pointing.

A metric has been created based on the above information for evaluating the success of the PSF subtraction, Figure 24. Arbitrary lines were drawn through the points that represent “good” PSF subtractions. The region between these lines represent favorable observing parameters, while those outside the “good” region would predict suspect PSF subtractions. This metric, though only for a few observations, indicates the trend stated above. This model does not include the corresponding roll of the telescope which could roll the NICMOS in and out of the HST shadow.

Based on this model, observations obtained in the “good” region of Figure 24 would yield subtraction images similar to n4nf15uwq-n4nf16v6q (Figure 20). Observations

obtained with observing parameters outside this region would yield “fair” or “poor” PSF subtractions.

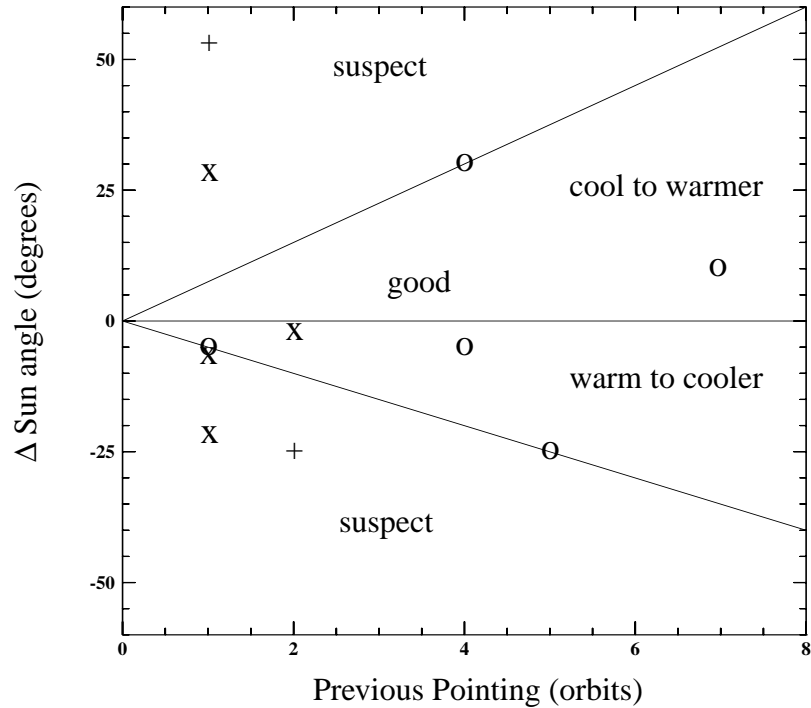


**Figure 24:** PSF subtraction metric. The region labeled “good” represents favorable observing parameters that would yield “good” PSF subtraction images. Regions outside the “good” region would yield “fair” or “poor” PSF subtraction images. Good PSF subtraction images are plotted with an “O”, a “fair” subtraction with an “x”, and a “poor” with a “+”.

This review is not intended to be an in-depth discourse on the thermal environment of NICMOS. However, it does indicate there is a possible time lag for PSF changes due to thermal input (cool to warmer), while there is a faster change to the PSF when slewing to smaller Sun angles (warm to cooler).

## 17. Appendix V - Co-addition of Coronagraphic Images

The **calnicb** task produces combined, or “mosaiced”, images from the image names contained in a NICMOS associated data set, the association table (`_asn.fits`). The task also performs background subtraction and source identification on the images in the association. When the images are shifted, to accomplish registration, a new shifted image is created and the new pixel values are combined. The interpolated pixel values are averaged with the regular values already at their respective locations in the first image.

Input to **calnicb** is the association table. The **calnicb** task parameter “`readoffsets=yes`” needs to be set to force **calnicb** to use the chosen offsets instead of computing its own. The following steps depicted illustrate a procedure to add the columns `XOFFSET` and `YOFFSET` to an existing association table and to use this table as input to **calnicb**. The IRAF task **tedit** within the `ttools` package was used to edit the association table.

```
> tedit n45j220b0_clean_asn.fits
```

```
ctl-D
```

```
Command: add column XOFFSET
Column type (r,d,i,s,b,ch*n)? r
Column print format? f8.3
Column units? pixel
```

Column	1	2	3	4
Label	MEMNAME	MEMTYPE	MEMPRSNT	XOFFSET
1	N45J22LAM_CL	EXP-TARG	yes	INDEF
2	N45J22LBM_CL	EXP-TARG	yes	INDEF
3	N45J22LCM_CL	EXP-TARG	yes	INDEF
4	N45J220B0_CL	PROD-TARG	yes	INDEF

```
ctl-D
```

```
Command: add column YOFFSET
Column type (r,d,i,s,b,ch*n)? r
Column print format? f8.3
Column units? pixel
```

Column	1	2	3	4	5
Label	MEMNAME	MEMTYPE	MEMPRSNT	XOFFSET	YOFFSET
1	N45J22LAM_CL	EXP-TARG	yes	INDEF	INDEF
2	N45J22LBM_CL	EXP-TARG	yes	INDEF	INDEF
3	N45J22LCM_CL	EXP-TARG	yes	INDEF	INDEF
4	N45J220B0_CL	PROD-TARG	yes	INDEF	INDEF

The table is edited by moving the cursor around the screen.

Column	1	2	3	4	5
Label	MEMNAME	MEMTYPE	MEMPRSNT	XOFFSET	YOFFSET
1	N45J22LAM_CL	EXP-TARG	yes	0.000	0.000
2	N45J22LBM_CL	EXP-TARG	yes	0.000	0.000
3	N45J22LCM_CL	EXP-TARG	yes	0.000	0.000
4	N45J220B0_CL	PROD-TARG	yes	INDEF	INDEF

```
Command: q
```

Write n45j220b0\_clean\_asn.fits? yes

```
> calnicb n45j220b0_clean_asn.fits readoffsets=yes
```